Lawrence Berkeley Laboratory
UNIVERSITY OF CALIFORNIA

Materials & Molecular Research Division

Presented at the NATO Advanced Study Institute on "Non-equilibrium Superconductivity, Phonons and Kapitza Boundaries", Maratea, Italy, August 25 - September 5, 1980; and to be published in the proceedings

CHARGE IMBALANCE

John Clarke

September 1980

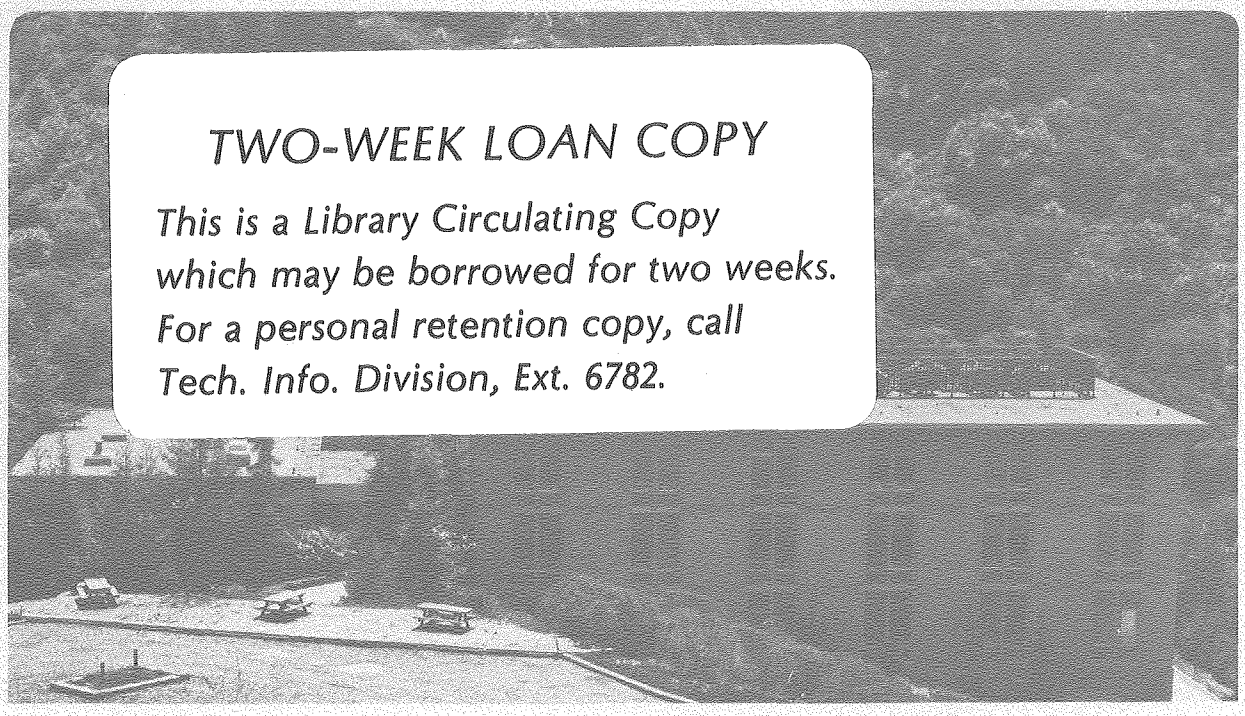

Prepared for the U.S. Department of Energy under Contract W-7405-ENG-48

DISCLAIMER

To be published in the proceedings of the
NATO Advanced Study Institute on "Non-equilibrium
Superconductivity, Phonons and Kapitza Boundaries"

LBL 11554

CHARGE IMBALANCE

John Clarke

Department of Physics, University of California and
Materials and Molecular Research Division, Lawrence
Berkeley Laboratory, Berkeley, California 94720

I. INTRODUCTION

If an electron-like ($k>k_F$) or a hole-like ($k<k_F$) excitation is added to a superconductor, a charge imbalance is created. Charge imbalance is of practical importance first, because it gives rise to a measureable steady-state voltage in a superconductor, and second, because it provides a tool for measuring various electron-relaxation rates. The importance of the disequilibrium of the electron- and hole-like branches was first pointed out by Pippard et al. (1971) who measured the electrical resistance of superconductor-normal metal-superconductor (SNS) sandwiches as a function of temperature. Near the superconducting transition temperature, T_c, they found that the resistance increased with increasing temperature. They ascribed this increase to the propagation of quasiparticles having a branch imbalance distribution into or out of the superconductor, a process that, at the time, they believed generated a potential step at each NS interface, and thus produced an additional boundary resistance. However, the first quantitative understanding of charge imbalance arose from experiments in which electrons were injected via a tunnel junction into a superconducting film (Clarke 1972); at the time this experiment was performed, its connection with the NS interface resistance was not apparent.

To motivate the long theoretical discussion that follows, we will begin by briefly reviewing the essential ideas of the tunneling experiment. The configuration used is shown in Fig. 1. First, a film of Al (XX') was deposited on a glass substrate and thermally oxidized, and a strip of Sn (YY') was evaporated at right angles to the first film to form a tunnel junction. The volume of Sn

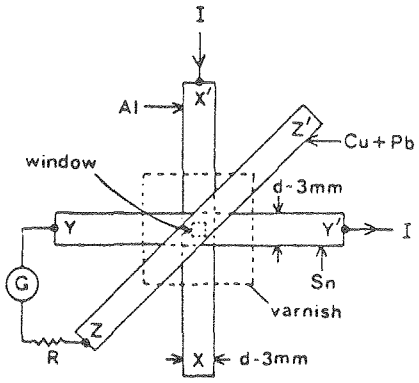

Fig. 1. Configuration of tunneling experiment to generate and detect charge imbalance in a Sn film. Galvanometer G (a SQUID) and resistor R are used to measure the voltage between the Sn and Cu films generated by the current passed between the Al and Sn films.

overlaying the Al was the region in which the charge imbalance was generated. The sample was removed from the evaporator, so that the Sn oxidized slightly, and a layer of varnish was applied leaving a window in the middle of the junction. A diagonal strip of Cu (ZZ') was evaporated to form the SIN junction that detects the charge imbalance. To reduce the resistance of the Cu strip, a film of Pb was deposited over it. With the sample immersed in liquid He^4, and with the Sn superconducting and the Al in the normal state, a current was passed between the Al and Sn films, and any voltage generated between the Sn and the Cu was measured with a SQUID voltmeter. A small voltage was detected that reversed sign when the sign of the injection current was reversed, and that was proportional to the injection current for injection voltages much higher than Δ/e, where $\Delta(T)$ is the energy gap in the Sn. The initial interpretation of this experiment by Tinkham and Clarke (1972) was later extended by Tinkham (1972) in a paper that laid the foundations of most of the important ideas of charge imbalance. Subsequently, there were two other theoretical papers of major importance, the first by Schmid and Schön (1975), who used a Green's function approach, and the second by Pethick and Smith (1979), who used a two-fluid approach involving the Boltzmann equation.

Charge imbalance has also been found to be central to several other experimental situations. In addition to the flow of current across an NS interface, these include the flow of a thermal current across an NS interface (Van Harlingen 1980), the resistance generated by phase slip centers in superconducting films (Skocpol et al., 1974), and the flow of supercurrent along a superconductor in which a thermal gradient exists (Clarke et al., 1979). The purpose of

this article is to review the theory of charge imbalance, and to discuss its relevance to a number of experimental situations. In Sec. II, we introduce the concepts of quasiparticle charge and charge imbalance, and discuss the generation and detection of charge imbalance by tunneling. In Sec. III we describe the relaxation of the injected charge imbalance by inelastic scattering processes, and show how the Boltzmann equation can be solved to obtain the steady state quasiparticle distribution and the charge relaxation rate. Section IV contains details of experiments to measure charge imbalance and the charge relaxation rate when inelastic scattering is the predominant relaxation mechanism. Section V is concerned with experiments on and theories of other charge relaxation mechanisms, namely relaxation via elastic scattering in the presence of energy gap anisotropy, or in the presence of a pair breaking mechanism such as magnetic impurities or an applied supercurrent or magnetic field. In Sec. VI we describe three other situations in which charge imbalance occurs, namely the resistance of the NS interface, phase slip centers, and the flow of a supercurrent in the presence of a temperature gradient. Finally, Sec. VII contains a concluding summary.

II. CHARGE IMBALANCE

In this section we introduce the concepts of quasiparticle charge and charge imbalance, and discuss the generation and detection of charge imbalance by tunneling. This discussion is based on the work of Tinkham and Clarke (1972), Tinkham (1972), Pethick and Smith (1979), Waldram (1975), and Kadin et al. (1980). These topics are also dealt with in detail by H. Smith in Chap. 15.

A. Quasiparticle Charge and Charge Imbalance

We begin by considering the total electronic charge, Q_{tot}, in a region of a superconductor, the overall charge at frequencies far below the plasma frequency being maintained at zero by the equal and opposite charge of the ion cores. From the BCS theory we have

$$Q_{tot} = \frac{2}{\Omega}\sum_k [u_k^2 f_k + v_k^2(1-f_{-k})], \tag{2.1}$$

where the sum is over k states above and below k_F, and the factor of 2 arises from the sum over spin. In Eq. (2.1), Ω is the volume of the superconductor, and f_k is the occupancy of the state $\vec{k}$, which, in thermal equilibrium, is the Fermi function. The u_k and v_k are the usual BCS factors given by

$$u_k^2 = \tfrac{1}{2}(1 + \xi_k/E_k) \tag{2.2}$$

and

$$v_k^2 = \tfrac{1}{2}(1 - \xi_k/E_k), \tag{2.3}$$

where

$$\xi_k = \hbar^2 k^2/2m - \mu_s \tag{2.4}$$

is the kinetic energy of the electron of mass m in the state $\vec{k}$ referred to the chemical potential of the superfluid, μ_s, and

$$E_k = (\Delta^2 + \xi_k^2)^{\frac{1}{2}} \tag{2.5}$$

is the quasiparticle excitation energy. In Eq. (2.5), $\Delta(T)$ is the energy gap of the superconductor. The energy E_k is positive for all values of k, while ξ_k is positive for $k>k_F$ and negative for $k<k_F$. Figure 2(a) shows u_k^2 and v_k^2 vs. ξ_k/Δ. The quantity v_k^2 is the probability that the state $\vec{k}$ is occupied by a Cooper pair, while $u_k^2 = 1 - v_k^2$ is the probability that the state $\vec{k}$ is not occupied by a Cooper pair. In thermal equilibrium we can readily interpret Eq. (2.1). The quantity in square brackets is the probability that the electron state $\vec{k}$ is occupied. The first term is the product of the probability that the pair state $(\vec{k},-\vec{k})$ be empty, u_k^2, and the probability that the quasiparticle state be occupied, f_k. The second term is the product of the probability that the pair state be filled, v_k^2, and the quasiparticle state $-\vec{k}$ be empty, $(1-f_{-k})$.

We can regard Eq. (2.1) as the sum of a superfluid contribution

$$Q_s = \frac{2}{\Omega}\sum_k v_k^2 \tag{2.6}$$

and a quasiparticle contribution

$$Q^* = \frac{2}{\Omega}\sum_k (u_k^2 - v_k^2) f_k \equiv \frac{2}{\Omega}\sum_k q_k f_k, \tag{2.7}$$

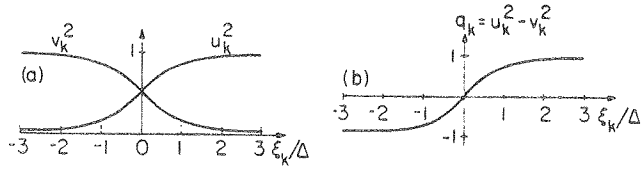

Fig. 2.(a) v_k^2 and u_k^2 vs. ξ_k/Δ and (b) q_k vs. ξ_k/Δ.

where we have set $f_{-k}=f_k$ in Eq. (2.1). In Eq. (2.7) we have introduced the very important concept of the effective quasiparticle charge

$$q_k \equiv u_k^2 - v_k^2 = \xi_k/E_k, \tag{2.8}$$

and defined the charge imbalance per unit volume, Q^*, which is the central subject of this paper. Figure 2(b) shows q_k vs. ξ_k; $q_k \to +1$ for $\xi_k >> \Delta$ ($k>k_F$), and $q_k \to -1$ for $\xi_k << -\Delta$ ($k<k_F$). It is evident in Eq. (2.7) that if $f_k(\xi_k)$ is the Fermi function, which is even in ξ_k about μ_s, the quasiparticle charge, Q^*, is zero since q_k is odd in ξ_k. Thus, the total electronic charge is $\frac{2}{\Omega}\Sigma v_k^2$ at all temperatures, as we expect.

We now turn to a non-equilibrium situation in which f_k is no longer the Fermi function. In this case, Q^* may be non-zero, and μ_s may be shifted from its equilibrium value, the Fermi energy, by an amount $\delta\mu_s$. As we shall see, Q^* and $\delta\mu_s$ are intimately related. As an example, suppose that we add excitations to the $k>k_F$ quasiparticle branch in a particular region of the superconductor. Overall charge neutrality will ensure that pairs with an equivalent charge are removed from the region. Thus, the chemical potential of the pairs must decrease by an amount $\delta\mu_s$, as indicated in Fig. 3(a). At the same time, the excitation spectrum shifts because its minimum still occurs at the pair chemical potential, as shown in Fig. 3(b). The effective quasiparticle charge is still $q_k = \xi_k/E_k$, but ξ_k is now referred to the shifted chemical potential, $\mu_s - \delta\mu_s$. Thus, the addition of a single electron-like excitation induces some quasiparticles near the bottom of the excitation spectrum to cross branches, and produces a small increase in the charge of all the electron-like quasiparticles, and a small decrease in the charge of all the hole-like quasiparticles.

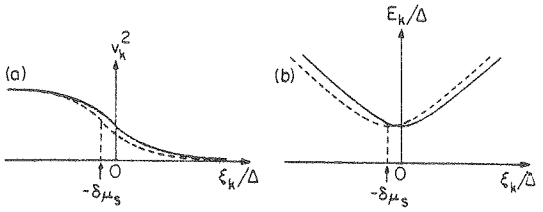

Fig. 3. The effect on (a) condensate density, and (b) the quasiparticle excitation spectrum when electron-like excitations are added to the superconductor. The solid and dashed lines represent equilibrium and the displacement from equilibrium, respectively.

The quantities Q^* and $\delta\mu_s$ are related as follows. By charge neutrality

$$Q^* + Q_s|_{\delta\mu_s \neq 0} = \frac{2}{\Omega}\sum_k v_k^2|_{\delta\mu_s=0} \quad , \tag{2.9}$$

or

$$Q^* = \frac{2}{\Omega}\sum_k (v_k^2|_{\delta\mu_s=0} - v_k^2|_{\delta\mu_s\neq 0}) \quad . \tag{2.10}$$

Now the reduction in the number of pairs represented by the right hand side of Eq. (2.10) is just $2N(0)\delta\mu_s$, where $N(0)$ is the single-spin density of states per unit volume at the Fermi energy. Thus

$$Q^* = -2N(0)\delta\mu_s. \tag{2.11}$$

We see that Eq. (2.1) is really a self-consistent equation for μ_s: Given any distribution, f_k, the constancy of Q_{tot} determines μ_s. This is somewhat analagous to the BCS gap equation, in which f_k determines $\Delta(T)$.

In steady state with Q^* continuously injected at a rate $\dot{Q}_i^*$, the excess distribution relaxes at a rate $\tau_{Q^*}^{-1}$ to produce a steady state charge imbalance Q^*. Thus

$$\tau_{Q^*}^{-1} = \dot{Q}_i^*/Q^*. \tag{2.12}$$

For the moment we shall regard $\tau_{Q^*}^{-1}$ as an empirical quantity, to be measured experimentally; we shall discuss its behavior in the presence of phonon scattering only in Sec. III, and contributions by other relaxation mechanisms in Sec. V.

To conclude our discussion on charge imbalance, it is instructive to consider qualitatively several disequilibrium situations. Figure 4(a) represents the addition of one excitation to the equilibrium distribution at some temperature. The quasiparticle charge, Q^*, is non-zero, as is the branch imbalance

$$Q = \frac{2}{\Omega}\left(\sum_{k>k_F} f_k - \sum_{k<k_F} f_k\right) \quad . \tag{2.13}$$

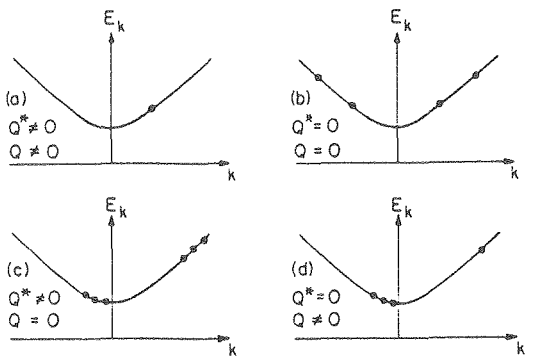

Fig. 4. Each dot represents a quasiparticle in excess of the equilibrium distribution: (a) $Q^*\neq 0$, $Q\neq 0$, (b) $Q^*=Q=0$, (c) $Q^*\neq 0$, $Q=0$, and (d) $Q^*=0$, $Q\neq 0$. In each case, the minimum value of E_k occurs at the pair chemical potential.

The quantity Q is the difference in the populations of the two branches, regardless of the effective charge, q_k. In Fig. 4(b), two excitations have been created on each branch in such a way that the net excitation population has been increased, but $Q^*=Q=0$. This is the so-called longitudinal mode of Schmid and Schön (1975). In Fig. 4(c), three quasiparticles have been added to each branch; thus $Q^*\neq 0$, because the excitations have different q_k, but $Q=0$. We note that this configuration of Q^* could relax if the quasiparticles on the $k>k_F$ branch scattered inelastically to lower energies; no inter-branch scattering is required. Finally, Fig. 4(d) shows a branch imbalance, $Q\neq 0$, with $Q^*=0$: The charge of the single $k>k_F$ quasiparticle (nearly unity) is sufficient to cancel exactly the charges of the three low-lying $k<k_F$ quasiparticles that are each less than unity.

B. Generation and Dectection of Charge Imbalance by Tunneling

We develop results for electron tunneling between a normal metal and a superconductor (NIS junction) that we can apply to both injection and detection processes. Single-particle tunneling is discussed at length by K. E. Gray in Chap. 5. We shall follow rather closely the approaches taken by Tinkham (1972) and Pethick and Smith (1979).

When a NIS junction is biased at a voltage V, the rate at which quasiparticles tunnel into the state $\vec{k}$ of the superconductor is given by a Golden Rule calculation:

$$\dot{f}_k\Big|_i = \frac{2\pi}{\hbar}\,|T|^2 \aleph_n(0)\{u_k^2(1-f_k)f^o(E_k-eV) - v_k^2 f_k[1-f^o(E_k+eV)]$$

$$-u_k^2 f_k[1-f^o(E_k-eV)] + v_k^2(1-f_k)f^o(E_k+eV)\}. \qquad (2.14)$$

Here, $|T|^2$ is the square of the tunneling matrix element, assumed to be independent of energy, and $\aleph_n(0)$ is the single-spin density of states in the volume of the metal. The Fermi functions $f^o(E_k \pm eV)$ refer to the normal metal, while f_k is the actual distribution in the superconductor, which is not, in general, the Fermi distribution. The four terms in braces in Eq. (2.14) correspond to the following processes respectively:

(i) An electron tunnels into the superconductor, creating an electron-like excitation with charge q_k; the remaining charge $(1-q_k)$ enters the condensate.

(ii) An electron tunnels into the superconductor, destroying a hole-like excitation, thus removing a charge q_k; the remaining charge $(1+q_k)$ enters the condensate.

(iii) An electron tunnels out of the superconductor, destroying an electron-like excitation and removing a charge q_k; the remaining charge $(-1+q_k)$ is supplied by the condensate [reverse of (i)].

(iv) An electron tunnels out of the superconductor, creating a hole-like excitation with charge q_k; the remaining charge $(-1-q_k)$ is supplied by the condensate [reverse of (ii)].

Cancelling some terms and using $u_k^2+v_k^2 = 1$, $u_k^2-v_k^2 = q_k$, we can rewrite Eq. (2.14) as

$$\dot{f}_k\Big|_i = \frac{2\pi}{\hbar}\,|T|^2 \aleph_n(0)[u_k^2 f^o(E_k-eV) + v_k^2 f^o(E_k+eV) - f_k]$$

$$= \frac{2\pi}{\hbar}\,|T|^2 \aleph_n(0)\{\tfrac{1}{2}[f^o(E_k+eV) + f^o(E_k-eV)] - f_k$$

$$+ \tfrac{1}{2}q_k[f^o(E_k-eV) - f^o(E_k+eV)]\}\,. \qquad (2.15)$$

In Eq. (2.15), we emphasize that q_k is given by ξ_k/E_k where ξ_k is defined relative to the actual pair chemical potential.

From Eq. (2.15) we can derive an expression for the rate of injection of charge. Charge is injected into the state $\vec{k}$ at the rate of $q_k \dot{f}_k|_i$. If we multiply Eq. (2.15) by q_k and sum over $\vec{k}$, noting that only the even terms contribute, we find

$$\dot{Q}_i^* = \frac{2\pi}{\hbar\Omega} |T|^2 \aleph_n(0) \sum_k q_k^2 [f^o(E_k-eV) - f^o(E_k+eV)]. \qquad (2.16)$$

The sum over spin produces a factor of 2 that cancels the factor ½ in Eq. (2.15). We have neglected the small contribution of the even part of $q_k f_k$ (i.e. we have neglected the odd part of f_k) on the grounds that the voltages generated by the non-equilibrium distribution are very small compared with the injection voltage. It is convenient to write Eq. (2.16) in integral form:

$$\dot{Q}_i^* = \frac{4\pi}{\hbar\Omega} |T|^2 \aleph_n(0)\aleph(0) \int_0^\infty \frac{\xi^2}{E^2} [f^o(E-eV) - f^o(E+eV)]d\xi$$

$$= \frac{G_{NN}}{e^2\Omega} \int_\Delta^\infty \rho^{-1}(E) \; [f^o(E-eV) - f^o(E+eV)]dE, \qquad (2.17)$$

where we have used $d\xi = (E/\xi)dE$. In Eq. (2.17), $\aleph(0)$ is the single-spin density of states in the volume of the superconductor when it is in the normal state, and $\rho(E) = E/(E^2-\Delta^2)^{\frac{1}{2}} = E/|\xi| = |q_k^{-1}| \quad (E>\Delta)$ is the normalized BCS density of states in the superconductor. We have introduced the conductance of the tunnel junction when the superconductor is in the normal state, $G_{NN} = 4\pi e^2 |T|^2 \aleph_n(0)\aleph(0)/\hbar$.

To obtain an expression for the net current injected into a superconductor from a normal metal, it is simplest to return to Eq. (2.14) and use the fact that the first two terms in braces add electrons to the superconductor, and make a positive contribution, while the last two terms remove electrons, and make a negative contribution. Summing over $\vec{k}$, after some simplification we find

$$I = \frac{4\pi e}{\hbar} |T|^2 \aleph_n(0) \sum_k [u_k^2 f^o(E_k-eV) - v_k^2 f^o(E_k+eV) - q_k f_k]. \qquad (2.18)$$

We now write $u_k^2 = \frac{1}{2}(1+q_k)$, $v_k^2 = \frac{1}{2}(1-q_k)$, and $f_k = f^o + \delta f_k$ to obtain*

*We note that the E_k in f^o are referred to the modified chemical potential. PS denote this f^o by $f^{o(l.e.)}$, where "l.e." means "local equilibrium;" our δf_k is precisely the same as their $\delta f_k^{l.e.}$.

$$I = \frac{2\pi e}{\hbar} |T|^2 \aleph_n(0) \sum_k [f^o(E_k - eV) - f^o(E_k + eV) - 2 q_k \delta f_k]. \qquad (2.19)$$

In deriving Eq. (2.19), we used the fact that $\Sigma[\frac{1}{2}f^o(E_k+eV) + \frac{1}{2}f^o(E_k-eV) - f^o(E_k)] = 0$. Note that $2 \Sigma q_k \delta f_k = 2 \Sigma q_k f_k = \Omega Q^*$, since the sum over the even part of f_k vanishes. For any injection voltage of practical interest the last term is negligible, and we can write I in the integral form:

$$I = \frac{4\pi e}{\hbar} |T|^2 \aleph_n(0) \aleph(0) \int_0^\infty [f^o(E-eV) - f^o(E+eV)] d\xi$$

$$= \frac{G_{NN}}{e} \int_\Delta^\infty \rho(E) [f^o(E-eV) - f^o(E+eV)] dE . \qquad (2.20)$$

We will find it useful to obtain an expression for Eq. (2.20) in the limit $eV << k_B T$ in which we can expand the Fermi functions to give $f^o(E \pm eV) = f^o(E) \pm (\partial f^o(E)/\partial E) eV$. This approximation leads to

$$I = G_{NN} \int_\Delta^\infty 2\rho(E) \left(- \frac{\partial f^o(E)}{\partial E} \right) V dE. \quad (eV << k_B T) \qquad (2.21)$$

Since the conductance, G_{NS} is just I/V, we obtain the useful result for the reduced tunneling conductance for $eV/k_B T \to 0$, $g_{NS}(0) = G_{NS}(0)/G_{NN}$:

$$g_{NS}(0) \equiv Y(T) = 2 \int_\Delta^\infty \rho(E) \left(- \frac{\partial f^o(E)}{\partial E} \right) dE, \qquad (2.22)$$

where Y(T) is the Yoshida function.

We are now in a position to calculate the voltage generated by the steady state charge imbalance as measured by a second tunnel junction with a normal metal. This voltage, V_d, referred to the chemical potential of the superconductor far away from the injected region where equilibrium obtains, is measured with zero current flowing through the detector junction. Since Eq. (2.19) is equally true for the injection and detection junctions, we can set I=0, and use the low-voltage expansion of the Fermi functions to obtain

$$V_d = \frac{2 \Sigma q_k f_k}{2e \Sigma(-\partial f^o(E)/\partial E)} = \frac{Q^*}{2N(0) e g_{NS}(0)} . \qquad (2.23)$$

We have thus found a simple relation between Q^* or, equivalently, $-2N(0)\delta\mu_s$, and the voltage measured by the detector junction. We note here that if, as is often the case, the detector junction does not show the ideal BCS behavior, one should use the measured normalized conductance in Eq. (2.23), rather than the BCS value.

To complete our description of tunneling generation and dectection of charge imbalance we need to combine Eqs. (2.12), (2.17), (2.20), and (2.23) so that we can deduce $\tau_{Q^*}^{-1}$ in terms of measureable or precisely calculable quantities. To do this, it is convenient to introduce the parameter F^* that enables us to express $\dot{Q}_i^*$ in terms of the injection current* I_i:

$$F^* = e\Omega\frac{\dot{Q}_i^*}{I_i} = \frac{\int_\Delta^\infty \rho^{-1}(E)[f^o(E-eV_i) - f^o(E+eV_i)]dE}{\int_\Delta^\infty \rho(E)[f^o(E-eV_i) - f^o(E+eV_i)]dE} . \qquad (2.24)$$

We have used V_i to denote the injection voltage. From Eqs. (2.12), (2.23) and (2.24) we find

$$\tau_{Q^*}^{-1} = \frac{\dot{Q}_i^*}{Q^*} = \frac{F^* I_i}{2N(0)e^2\Omega g_{NS}(0)V_d} . \qquad (2.25)$$

The quantity F^* is readily calculable, while the quantities I_i, Ω, $g_{NS}(0)$, and V_d are the quantities measured in the experiment.

In the limit of low injection voltages, $eV_i << k_BT$, the Fermi functions in Eq. (2.24) may be expanded to yield

$$F^* = Z(T)/Y(T), \quad (eV_i << k_BT) \qquad (2.26)$$

---

*It is evident that the integral expression for $\dot{Q}_i^*$ is less than that for I_i by a factor of $(\xi/E)^2$. To understand this, consider an electron injected at an energy $\sim\Delta$. Since the electron has a nearly equal probability of producing a quasiparticle on the $k_>$ and $k_<$ branches, the distribution imbalance is reduced by one factor of ξ/E. The second factor of ξ/E arises from the reduction in quasiparticle charge at low energies.

where $Z(T) \equiv 2 \int_{\Delta}^{\infty} \rho^{-1}(E) \left(- \frac{\partial f^{o}(E)}{\partial E} \right) dE.$ (2.27)

However, this limit is not very useful for most practical experiments with tunneling injections which are performed at injection voltages large compared with both $\Delta(T)/e$ and $k_B T/e$ (see Sec. IV). In these limits, one obtains

$$F^{*} = 1 - \pi\Delta/2|eV_i| \quad (eV_i >> k_B T,\ eV_i >> \Delta(T)) \tag{2.28}$$

For a typical injection voltage, $eV_i/\Delta = 30$, we find $F^{*} = 0.95$.

At this point we have developed the ideas and results necessary to interpret a tunneling experiment that measures $\tau_{Q^*}^{-1}$. However, we shall continue our theoretical development, and in Sec. III discuss the form of the injected distribution, and the dependence of $\tau_{Q^*}^{-1}$ on injection voltage and temperature for the case in which relaxation is via phonon scattering only.

III. CHARGE RELAXATION AND QUASIPARTICLE DISTRIBUTION FUNCTION IN THE PRESENCE OF PHONON SCATTERING

A. Introduction

When an electron-like excitation (for example) is injected into the superconductor, in general it not only creates a charge imbalance but also carries an energy well above thermal energies. Thus the processes that restore equilibrium involve both cooling and charge relaxation. However, these are not necessarily distinct processes. For example, if the quasiparticle is initially at an energy considerably above both $\Delta(T)$ and $k_B T$, it may emit a phonon and scatter on the same branch to an energy not too much greater than $\Delta(T)$. Clearly, the quasiparticle has cooled; in addition, it has given up some of its charge because $q(\equiv q_k)$ has been reduced from an initial value close to unity to a lower value. In this introductory discussion we shall not concern ourselves with cooling processes, but rather confine our attention to a qualitative discussion of charge relaxation that hopefully will set the scene for the quantitative description that follows in Sect. III B. Initially, we restrict ourselves to the temperature range near T_c where $\Delta/k_B T << 1$, and to a consideration of inelastic processes only. There are several calculations (Tinkham 1972, Schmid and Schon 1975, Pethick and Smith 1979) of the charge relaxation rate under these conditions,

all leading to the result*

$$(F^{*}\tau_{Q}^{*})^{-1} = (\pi\Delta/4k_{B}T)\ \tau_{E}^{-1} \quad . \tag{3.1}$$

In Eq. (3.1), τ_{E}^{-1} is the inelastic scattering rate at T_{c} for a quasiparticle at the Fermi energy; the rate actually increases with the energy of the quasiparticle, but we shall neglect this dependence for the moment. A charge imbalance may relax through both quasiparticle scattering and recombination, and we now discuss these processes, giving qualitative arguments for Eq. (3.1).

We make the rather crude simplifying assumption that there are excess quasiparticles on the $k>k_{F}$ branch uniformly distributed in energy from Δ to $k_{B}T$. Consider first the scattering of a quasiparticle with energy $\sim k_{B}T$. This quasiparticle may scatter with the emission or absorption of a phonon with energy $\hbar\Omega$ to a new state E' on either the $k>k_{F}$ or the $k<k_{F}$ branch. The maximum phonon energy available for absorption is $\sim k_{B}T$. The coherence factor that governs these processes (Tinkham 1975) is

$$(uu'-vv')^{2} = \tfrac{1}{2}\left(1 + \frac{\xi\xi'-\Delta^{2}}{EE'}\right) \quad . \tag{3.2}$$

Suppose E' is on the $k>k_{F}$ branch [Fig. 5(a)]. Since ξ, ξ' are both positive and $E\sim k_{B}T_{c} >> \Delta$, the coherence factor is substantial for any value of E'. However, upward transitions, with phonon absorption, do not change q significantly, while downward transitions, with phonon emission, change q significantly only when $\Delta \lesssim E' \lesssim 2\Delta$ (say). Thus, of all possible transitions of this nature, only a fraction $\sim\Delta/2k_{B}T$ can relax Q* significantly. Next, consider scattering onto the $k<k_{F}$ branch [Fig. 5(b)]. Given that $E \approx \xi >> \Delta$, we see that if $E' >> \Delta$ so that $\xi' \approx -E'$, the coherence factor is essentially zero. Thus, scattering to energies E' higher than E is rare. Moreover, scattering to energies lower than E is likely only if E' is reasonably close to Δ, say, between Δ and 2Δ; at $E'=2\Delta$, the coherence factor is $\approx \tfrac{1}{2}(1 - \sqrt{3}/2) \approx 0.07$. Thus, again, only a fraction $\sim\Delta/2k_{B}T$ of transitions relax Q^{*}. We can extend our arguments to an injected $k>k_{F}$ electron in the range Δ to $\sim 2\Delta$, to find that it can scatter (upwards) into an energy range $\sim k_{B}T$ with significant change

*The paper by Tinkham (1972) contains a numerical error of order unity that was corrected in ref. 10 of Clarke et al. (1979).

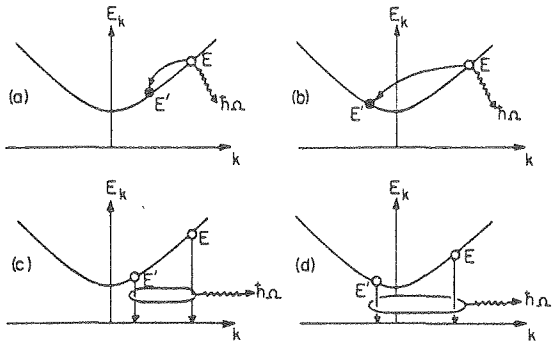

Fig. 5. Four inelastic processes that contribute to the relaxation of the charge of a quasiparticle with energy E. (a) scattering to a state of lower charge on the $k>k_F$ branch; (b) scattering to a state of lower charge of opposite sign on the $k<k_F$ branch; (c) recombination with a quasiparticle near the gap edge on the $k>k_F$ branch; (d) recombination with a quasiparticle near the gap edge on the $k<k_F$ branch. Processes (a) and (b) are governed by the coherence factor $(uu'-vv')^2$, while (c) and (d) are governed by the coherence factor $(vu'+uv')^2$.

of q. Clearly, a fraction $\sim\Delta/k_BT$ of the excess quasiparticles relax their charge in this way. We conclude that the overall charge relaxation rate for phonon scattering is $\tau_{Q^*}^{-1} \sim(\Delta/k_BT)\ \tau_E^{-1}$.

We note in passing that elastic scattering from non-magnetic impurities can only relax Q^* if the quasiparticle changes branches. In an isotropic superconductor, this process is strictly forbidden by the coherence factor Eq. (3.2), as can be seen immediately by realizing that if E and E' refer to different branches, u'=v, and v'=u. Consequently, it is perfectly reasonable to consider a theory in which only inelastic processes relax Q^*. Later, in Sec. V, we discuss elastic scattering in an anisotropic superconductor, and also elastic scattering from magnetic impurities. For the moment, elastic scattering merely serves to scatter injected quasiparticles uniformly around the Fermi surface on the same branch without affecting the value of Q^*.

We now turn our attention to Q^* relaxation by recombination, a process that is governed by the coherence factor (Tinkham 1975)

$$(vu'+uv')^2 = \tfrac{1}{2}\left(1 + \frac{\Delta^2-\xi\xi'}{EE'}\right), \tag{3.3}$$

where E is the energy of the quasiparticle under consideration, and E' is the energy of the quasiparticle with which it recombines. First, consider recombination when E and E' refer to the same branch [Fig. 5(c)]. If E, E' are both large compared with Δ, the coherence factor becomes very small. However, if one energy is not too great, no greater than 2Δ, say, the coherence factor is relatively large, and recombination can make a substantial contribution to charge relaxation. A fraction $\sim\Delta/k_BT$ of the quasiparticles can relax Q^* in this way. Now consider recombination with E and E' on different branches [Fig. 5(d)]. Since the product $-\xi\xi'$ is now positive, the coherence factor is always at least $\frac{1}{2}$. However, recombination processes have little effect on Q^* for energies where $|q|$ is reasonably close to unity. When one quasiparticle lies between Δ and $\sim 2\Delta$, and the other is at higher energies, Q^* does relax significantly, such processes representing a fraction $\sim\Delta/k_BT$ of the total. We conclude that recombination events again lead to an overall charge relaxation rate $\sim(\Delta/k_BT)\ \tau_E^{-1}$.

These qualitative arguments give some insight into the temperature dependence of $\tau_{Q^*}^{-1}$ near T_c. However, one is usually interested in a much wider temperature range, and, further, one would like to know the form of the steady state non-equilibrium distribution. To extend the theory one must resort to a numerical solution of the Boltzmann equation, which is the subject of Section III B.

B. The Boltzmann Equation for Charge Relaxation

This section follows closely the work of Chi and Clarke (1979, 1980) (CC). The Boltzmann equation simply expresses the total rate at which quasiparticles are injected into and scatter into and out of the state ξ_k, and can be written in the form

$$\dot{f}_\xi = G_\xi - G_{in\xi} - G_{el\xi} \ . \tag{3.4}$$

The first term G_ξ is the rate of injection into ξ_k, while $G_{in\xi}$ and $G_{el\xi}$ are the inelastic and elastic rates at which quasiparticles scatter out of ξ_k; for the moment we set $G_{el\xi}=0$. In a steady state situation $\dot{f}_\xi=0$. For tunneling from a normal metal into a superconductor the injection rate is given by the first line of Eq. (2.15) with the terms labeled with ξ rather than $\vec{k}$:

$$G_\xi = R_o\{\tfrac{1}{2}(1+\xi/E)[f^o(E-eV_i)-f^o(E)]-\tfrac{1}{2}(1-\xi/E)[f^o(E)-f^o(E+eV_i)]\}, \tag{3.5}$$

where

$$R_o \equiv G_{NN}/2N(0)e^2\Omega \ . \tag{3.6}$$

We have used the Fermi distribution for the distribution functions, thereby assuming the departure from equilibrium is small.

The inelastic scattering rate is proportional to $\alpha^2F(\Omega)$, the average of the product of the square of the matrix element for the electron-phonon interaction and the phonon density of states. We assume that $F(\Omega)$ is quadratic in Ω, and can be written in the form $F(k_BT_c/\hbar)(\Omega/k_BT_c)^2$. With this assumption, $G_{in\xi}$ can be written down using the Golden Rule (Kaplan et al. 1976, Chang and Scalapino 1977, Chang 1979, CC):

$$G_{in\xi} = \frac{2\pi}{\hbar}\frac{\alpha^2F(k_BT_c/\hbar)}{Z_1(0)(k_BT_c)^2}\int_{-\infty}^{\infty}d\xi' \ \times$$

$$\left[\tfrac{1}{2}\left(1-\frac{\xi\xi'}{EE'}+\frac{\Delta^2}{EE'}\right)(E+E')^2\{[1+n^o(E+E')]f_\xi f_{\xi'}-n^o(E+E')(1-f_\xi)(1-f_{\xi'})\}\right.$$

$$+\tfrac{1}{2}\left(1+\frac{\xi\xi'}{EE'}-\frac{\Delta^2}{EE'}\right)(E-E')^2\Theta(E-E')\{[1+n^o(E-E')]f_\xi(1-f_{\xi'})-n^o(E-E')f_{\xi'}(1-f_\xi)]\}$$

$$\left.+\tfrac{1}{2}\left(1+\frac{\xi\xi'}{EE'}-\frac{\Delta^2}{EE'}\right)(E-E')^2\Theta(E'-E)\{n^o(E'-E)f_\xi(1-f_{\xi'})-[1+n^o(E'-E)]f_{\xi'}(1-f_\xi)\}\right]. \tag{3.7}$$

In Eq. (3.7), $Z_1(0)$ is the electron-phonon renormalization factor, typically about 2 for most metals, Θ is the Heaviside function, which is zero for negative arguments and unity for positive arguments, and $n^o(\Omega)$ is the Bose-Einstein distribution function for the phonons. The first and second lines represent recombination, and contain a matrix element squared, a phonon density of states proportional to Ω^2, a coherence factor [Eq. (3.3)], and various quasiparticle and phonon occupation numbers. The first term in braces represents recombination with phonon emission, while the second represents the reverse process, pair breaking, with phonon absorption. Since E and E' cannot be less than Δ, the phonon energies involved are all $>2\Delta$. The first and third lines represent phonon scattering between E and states $E'<E$, and again contain a matrix element squared, a phonon density of states, a coherence

factor [Eq. (3.2)], and various quasiparticle and phonon occupation numbers. The first term in braces represents scattering to lower energy states with phonon emission, while the second represents the reverse process, with phonon absorption. The first and fourth lines represent scattering between state E and states E'>E.

In Eq. (3.7), we have assumed that the phonons are in thermal equilibrium. Because of phonon trapping (Rothwarf and Taylor 1967), this is not a good approximation if one is interested in the total excess quasiparticle density. However, it is a valid approximation for the calculation of Q^* because the trapped excess phonons break pairs that on the average populate the two branches equally, and do not therefore affect the value of Q^*. We have also used the thermal equilibrium value of the energy gap, thereby assuming that the deviation from thermal equilibrium is very small.

The inelastic scattering rate, τ_E^{-1}, can be written in the form (Kaplan et al. 1976)

$$\tau_E^{-1} = \frac{14\zeta(3)\pi k_B T_c \alpha^2 F(k_B T_c/\hbar)}{\hbar Z_1(0)} , \tag{3.8}$$

so that the prefactor of the integral in Eq. (3.7) is just $1/7\zeta(3)(k_B T_c)^3 \tau_E$.

C. Computer Solution of the Boltzmann Equation

It is convenient to write the quasiparticle distribution function as $f_\xi = f^o + \delta f_\xi$ (remembering that ξ is referred to the shifted chemical potential), where f^o is the Fermi function at energy $(\xi^2+\Delta^2)^{1/2}$. We then rewrite the Boltzmann equation in terms of the even (longitudinal) and odd (transverse) components of δf_ξ, $\delta f_\xi^L = \frac{1}{2}(\delta f_\xi + \delta f_{-\xi})$ and $\delta f_\xi^T = \frac{1}{2}(\delta f_\xi - \delta f_{-\xi})$. We make an initial guess at the values of δf_ξ^L and δf_ξ^T for values of ξ from zero to some energy much larger than the largest of Δ, $k_B T$, and $|eV_i|$, and use the Boltzmann equation to generate new values of δf_ξ^L and δf_ξ^T. This procedure is iterated until we find a consistent solution. We calculate Q^* from $4N(0)\Sigma q_\xi \delta f_\xi^T$, and find $\tau_{Q^*}^{-1}$ from $\dot{Q}_i^*/Q^*$, using Eq. (2.17).

D. Computed Distribution Function

In Fig. 6 (from CC 1980) we plot $\delta f_>(E) - \delta f_<(E)$ vs. $\Delta(T)/k_B T$ for $V_i = 0.01\ \Delta(T)/e$ and $T/T_c = 0.99$ and 0.9, where $\delta f_{\gtrless}(E)$ represents

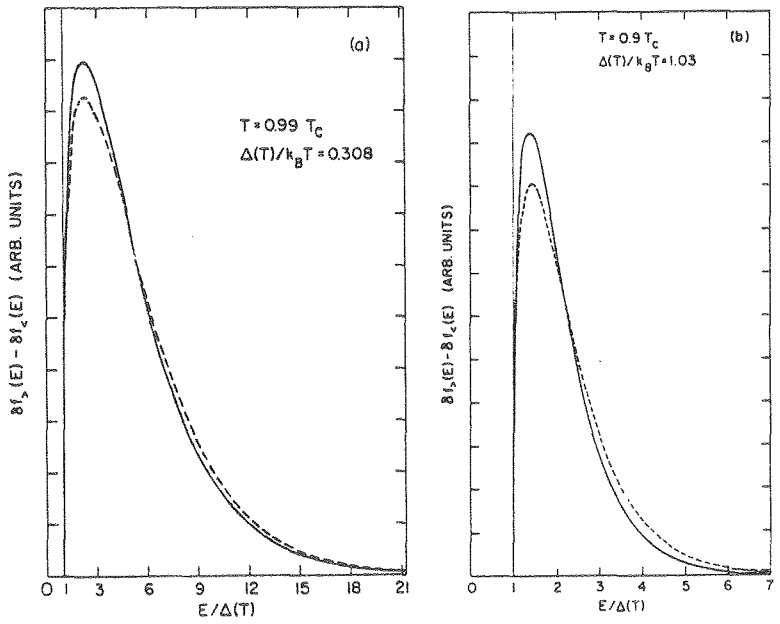

Fig. 6. $\delta f_>(E) - \delta f_<(E)$ vs. $E/\Delta(T)$ at (a) $T=0.99T_c$, and (b) $T=0.9T_c$: ——— computer calculation with $V_i=0.01\Delta(T)/e$, and - - - - Pethick-Smith chemical potential model. Both curves are normalized to give the same value of Q*.

the deviation from equilibrium for $k \gtrless k_F$. The rapid decrease in the distribution below $\sim 2\Delta(T)$ as $E/\Delta(T) \to 1$ is due to the reduced generation rate at low energies described in Sec. IIB. The roll-off at high energies reflects the decrease in the injected distribution with increasing energy. At this very low injection voltage, electrons are injected almost equally into the $\vec{k}_>$ and $\vec{k}_<$ branches, so that the increase in the number of $\vec{k}_>$ quasiparticles is very nearly equal to the decrease in the number of $\vec{k}_<$ quasiparticles. Thus, the net number of quasiparticles is essentially unchanged (i.e. the longitudinal mode is not excited). In this limit, the chemical potential model of Pethick and Smith (1979) is expected to be a good description of the distribution. In their model, remembering that $E = [\Delta^2 + (\xi - \mu_s)^2]^{\frac{1}{2}}$, we can write the change in the distribution as

$$\delta f = \frac{\partial f^o}{\partial E} \frac{\partial E}{\partial \mu_s} \delta\mu_s = - \frac{\partial f^o}{\partial E} \frac{\xi}{E} \delta\mu_s, \qquad (3.9)$$

so that

$$(\delta f_{>} - \delta f_{<}) = 2\left(-\frac{\partial f^{o}}{\partial E}\right)\frac{|\xi|}{E}\,\delta\mu_{s}. \qquad (3.10)$$

This result is also shown in Figs. 6(a) and (b), normalized to represent the same value of Q^* as the computed curve. The chemcial potential curve is slightly lower than the computed distribution near the peak, and slightly higher at energies above about $6\Delta(T)$ and $2\Delta(T)$ for $T/T_c=0.99$ and 0.9 respectively.

In Fig. 7 (CC 1980) we plot the computed curves at $V_i=0.01\times\Delta(T)/e$ and $20\Delta(T)/e$ for $T/T_c=0.9$. Both curves have been normalized to give the same value of Q^*. Injection at the higher voltages leaves the position of the peak virtually unchanged, but shifts part of the distribution from under the peak into the high energy tail. This shift indicates that some of the initial quasiparticles cross to the other branch as they cool from their high initial energy.

E. Voltage and Temperature Dependence of $\tau_{Q^*}^{-1}$

In the limit $T\to T_c$, theory predicts that to first order in $\Delta(T)/k_BT$, $\tau_{Q^*}^{-1} = (\pi\Delta(T)/4k_BT)\tau_E^{-1}$. To test the accuracy of this

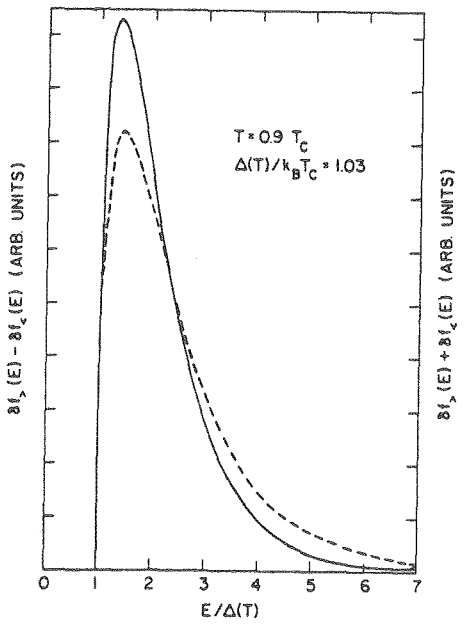

Fig. 7. $\delta f_{>}(E) - \delta f_{<}(E)$ vs. E/k_BT at $T=0.9T_c$: ——— $V_i=0.01\Delta(T)/e$, and - - - $V_i=20\Delta(T)/e$. Both curves are normalized to give the same value of Q^*.

result at temperatures below T_c, CC computed $\tau_{Q^*}^{-1}$ for $eV_i=0.01\Delta(T)$, $10\Delta(T)$, and $10k_BT_c$; the results are plotted in Fig. 8 (from CC 1980). At T_c, the computed values agree precisely with the theoretical values for all three injection voltages. However, as the temperature is lowered from T_c, $\tau_{Q^*}^{-1}\,[4k_BT\tau_E/\pi\Delta(T)]$ initially increases and then decreases, the exact form of the curve depending on the injection voltage. At all temperatures below T_c, $\tau_{Q^*}^{-1}$ increases with increasing injection voltage. This behavior reflects the increase in the inelastic scattering rate with increasing energy that is evident in the distribution of Fig. 7; inspection of Eq. (3.7) shows that the inelastic scattering rate out of a given state of energy E increases as E^3. In the low voltage limit and for $\Delta(T)/k_BT \leqslant 0.6$, CC found that the computed curve could be fitted to within ±1% by the empirical formula

$$\frac{\tau_{Q^*}^{-1}4k_BT\tau_E}{\pi\Delta} = 1 + \tfrac{1}{2}\left(\frac{\Delta}{k_BT}\right) - \frac{3}{4}\left(\frac{\Delta(T)}{k_BT}\right)^2 . \quad (eV_i \ll \Delta(T), \quad \Delta(T)/k_BT \leqslant 0.6) \tag{3.11}$$

CC also computed the temperature dependence of $\tau_{Q^*}^{-1}$ predicted by the Pethick-Smith distribution, Eq. (3.9), using the following procedure: (i) δf_ξ from Eq. (3.8) is used in Eq. (3.7) to calculate $G_{in\xi}$; (ii) the values of $G_{in\xi}$ are used in Eq. (3.4) to calculate G_ξ; (iii) the values of G_ξ are used to calculate Q_i^* from

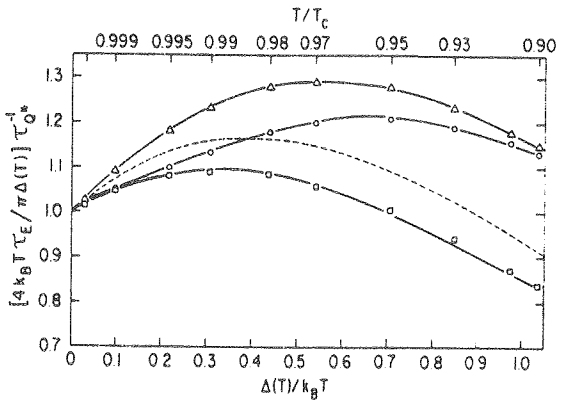

Fig. 8. $(4k_BT\tau_E/\pi\Delta)\tau_{Q^*}^{-1}$ vs. $\Delta(T)/k_BT$ and T/T_c: Computed values for $eV_i=0.01\Delta(T)$ (—□—), $10\Delta(T)$ (—○—), and $10k_BT_c$ (—Δ—); Pethick-Smith model (- - - -).

$\dot{Q}_i^*$ $= \int_0^\infty d\xi(\xi/E)(G_\xi - G_{-\xi})$; (iv) $\tau_{Q^*}^{-1}$ is found from $\dot{Q}_i^*/Q^*$. The result is shown as the dashed line in Fig. 8. At temperatures below T_c, the PS value of $\tau_{Q^*}^{-1}$ lies roughly 10% above the computed value for low injection voltages. This result can be understood by inspection of the distribution in Fig. 6. Since the PS distribution contains less quasiparticle charge near the peak and more at high energies than the computed distribution, it necessarily relaxes more rapidly because the inelastic scattering rate increases with energy.

The computed temperature dependence of $\tau_{Q^*}^{-1}$ is shown in Fig. 9 at temperatures down to $0.3T_c$ for $eV_i = 0.01\Delta(T)$ and $10\Delta(T)$, together with the PS prediction. As the temperature is lowered from T_c, the rate goes through a peak at a temperature that depends on the injection voltage, and then decreases steadily. The PS value always lies slightly above the low-injection voltage curve. It should be emphasized that these curves are computed only for inelastic-scattering processes, and that in real superconductors

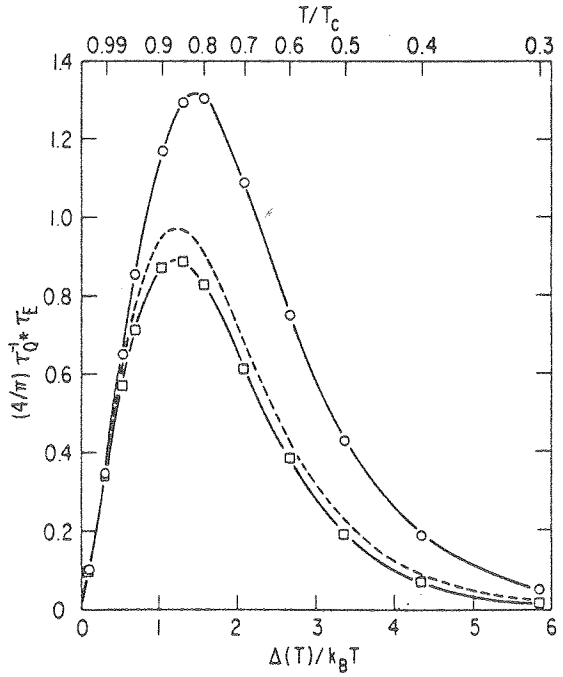

Fig. 9. Computed values of $(4/\pi)\tau_{Q^*}^{-1}\tau_E$ vs. $\Delta(T)/k_BT$ and T/T_c for $eV_i = 0.01\Delta(T)$ (—□—), and $10\Delta(T)$ (—○—); dashed line is PS model.

elastic scattering in the presence of an anisotropic energy gap is likely to increase the low-temperature value of $\tau_{Q^*}^{-1}$ very substantially (see Sec. V).

Finally, Fig. 10 shows $\tau_{Q^*}^{-1}$ and $(F^*\tau_{Q^*})^{-1}$, normalized to $\pi\Delta(T)/4k_BT\tau_E$, vs. $eV_i/\Delta(T)$ at $T=0.9T_c$. The experimentally measured voltage V_d is directly proportional to $(F^*\tau_{Q^*})I_i$. We see that for $V_i \gtrsim 6\Delta(T)/e$ the voltage dependences of τ_{Q^*} and F^* cancel, so that $F^*\tau_{Q^*}$ becomes independent of voltage, and V_d becomes linear in I_i, as is observed experimentally (see Sec. IV).

This concludes our discussion of the theory of the relaxation of charge imbalance via inelastic scattering. We now move on to describe experimental measurements of Q^* and $\tau_{Q^*}^{-1}$.

IV. EXPERIMENTAL MEASUREMENTS OF Q* AND $\tau_{Q^*}^{-1}$ IN TIN

We begin our description of the experimental work with measurements on Sn (Clarke 1972, Clarke and Paterson 1974, Moody and Paterson 1979) because in this material it is possible to obtain an identificable temperature range near T_c in which inelastic charge relaxation dominates the elastic charge relaxation that is allowed in the presence of an anisotropic energy gap. A discussion of the latter process is deferred until Section VA. In this section we confine our discussion to the measurements by Clarke and Paterson (1974).

The basic configuration used in all tunneling injection experiments is shown in Fig. 1. Usually, four junctions were made simul-

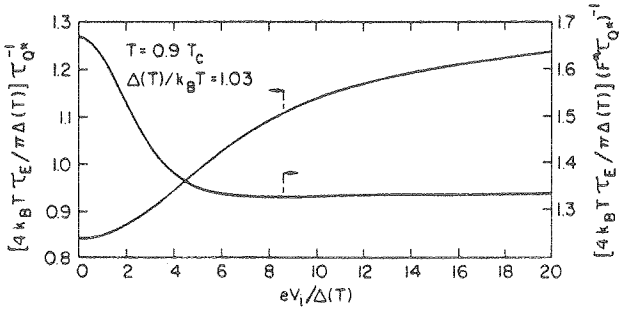

Fig. 10. $[4k_BT\tau_E/\pi\Delta(T)]\tau_{Q^*}^{-1}$ and $[4k_BT\tau_E/\pi\Delta(T)](F^*\tau_{Q^*})^{-1}$ vs. $eV_i/\Delta(T)$ for $T=0.9T_c$.

taneously. First, an Al film (XX') 120 to 200 nm thick and 3mm wide was evaporated through a metal mask onto a glass substrate. The Al was thermally oxidized in the evaporator, and a 3-mm wide cross strip of Sn(YY') 200 to 400 nm thick was deposited to complete the injector junction. The Sn film was then exposed to the atmosphere for 20 minutes to 2½h to produce a thin oxide barrier. The substrate was returned to the evaporator, and SiO deposited to mask off a $1 \times 1 mm^2$ window near the middle of the injector junction (SiO replaced varnish in all but the earliest measurements). A diagonal strip (ZZ') of CuAl (3 wt.%Al) about 2 μm thick was evaporated to make contact with the Sn oxide through the window in the SiO: This forms the detector junction. Because the rather high series resistance of the CuAl strip ($\gtrsim 1\Omega$) would have greatly reduced the voltage resolution, a Pb film was deposited over the CuAl. The Al in the Cu reduced the mean free path, ℓ, to $\sim$10nm, and thereby reduced the pair decay length, $(\hbar v_F \ell / 6\pi k_B T)^{1/2}$, sufficiently to eliminate Josephson tunneling between the Sn and Pb films (de Gennes 1964). The CuAl films were deposited by flash evaporation of pellets from a tungsten boat. The film thicknesses were monitored with a quartz crystal microbalance during evaporation; the thickness of each Sn strip was checked with an optical interferometer after completion of the electrical measurements.

The Sn-SnOx-CuAl+Pb junctions of the four samples on each substrate were connected in series with a calibrated resistor, R, and a superconducting coil coupled to a SQUID (see, for example, Clarke 1976). The output from the SQUID, suitably amplified, was fed back across the resistor R to produce negative feedback. Thus, any voltage developed across one of the detector junctions was measured at zero current, as required by Eq. (2.23). The circuit was carefully shielded to minimize the effects of fluctuating external fields, and of vibrations in static fields. The earth's magnetic field was reduced by about two orders of magnitude by means of two conductive μ-metal shields around the cryostat. A superconducting shield surrounded the low-temperature circuit, which was immersed directly in liquid helium. At temperatures below the λ-point the limiting noise in the measurement was determined by the Johnson noise developed in the probe junctions and the series resistor. Above the λ-point, the rms noise was several times greater, and probably arose from thermoelectric voltages developed by fluctuating temperature gradients in the bath.

We investigated each sample independently by connecting a current to the appropriate terminals. First, we obtained the $I_i - V_i$ characteristic of the injector junction by applying a current to X'Y' and measuring the voltage across XY. Next, we measured the resistance of the probe junction at low voltages by applying a current to Y'Z' and measuring the voltage across YZ with the SQUID voltmeter. Last, we measured the non-equilibrium voltage across YZ with the SQUID as a function of the injection current I_i.

The Al-AlOx-Sn injection junctions were of high-quality with a typical resistance of 1Ω at voltages above the energy gap. The Sn-SnOx-CuAl detector junctions had a resistance of typically $10^{-5}\Omega$ at the transition temperature of the Sn. From the variation of resistance with temperature, one can obtain measured values of $g_{NS}(0)$. Figure 11 shows typical measured values of $g_{NS}(0)$ for 4 samples together with the behavior predicted by Eq. (2.22). In general the conductances lie above the theoretical value, often by a substantial amount. However, it was found that if one used the measured value of $g_{NS}(0)$ to compute $\tau_{Q^*}^{-1}$ using Eq. (2.25), the values of $\tau_{Q^*}^{-1}$ obtained from different samples at a given temperature and injection voltage agreed well with each other. Thus, it appears that the quality of the detector junction is not a vital factor in the determination of $\tau_{Q^*}^{-1}$; however, the barrier between the Sn and the CuAl must be sufficient to quench the proximity effect (DeGennes 1964) that would otherwise depress the order parameter in the superconductor. Very near T_c the conductance often dropped by a few percent with increasing temperature. This decrease in conductance is believed to arise from the resistance experienced by the quasiparticles injected into the superconductor, just as in the case of the excess resistance observed at the NS interface (see Sec. VA). The

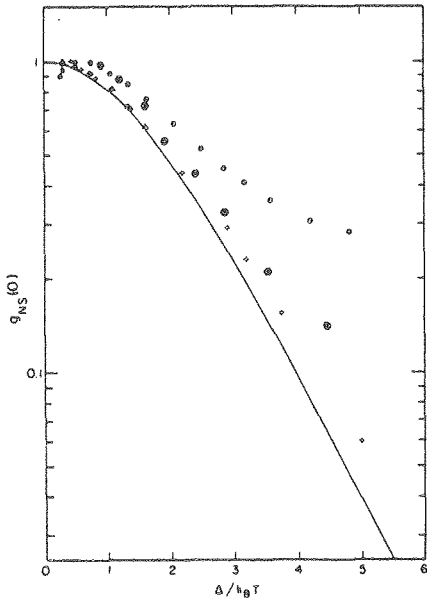

Fig. 11. Measured values of $g_{NS}(0)$ vs. Δ/k_BT for three Sn-SnOx-Cu (● ▲ +) and one SnIn-SnOx-Cu (✱) detector junctions compared with theory (solid line).

conductance dip is observed in these junctions because the resistance of the barrier is so low; for junctions with resistances of (say) 1mΩ or higher, the effect would be unobservably small. Since the excess resistance occurs only very close to T_c, the values of the conductance well below T_c were normalized to the maximum value of the conductance, rather than to the value at T_c.

At each temperature V_d was plotted vs. I_i for both polarities of the injection current. Near T_c, the values of V_d/I_i for both polarities were almost equal, but at lower temperatures there was often a marked asymmetry. This asymmetry probably arose from thermoelectric voltages generated by thermal gradients induced by heating in the injection junction [see Moody and Paterson (1979) for a discussion]. Provided the asymmetry is not too large, one can eliminate it in the data analysis by averaging together the two values of V_d/I_i. In the present analysis we confine our attention to high injection voltages, where $F^* \sim 1$.

For each sample one computes $g_{NS}(0)\Omega V_d/I_i = F^*\tau_{Q^*}/2N(0)e^2$. The results for $V_i = 10\Delta(T)/e$ are plotted in Fig. 12 for three sets

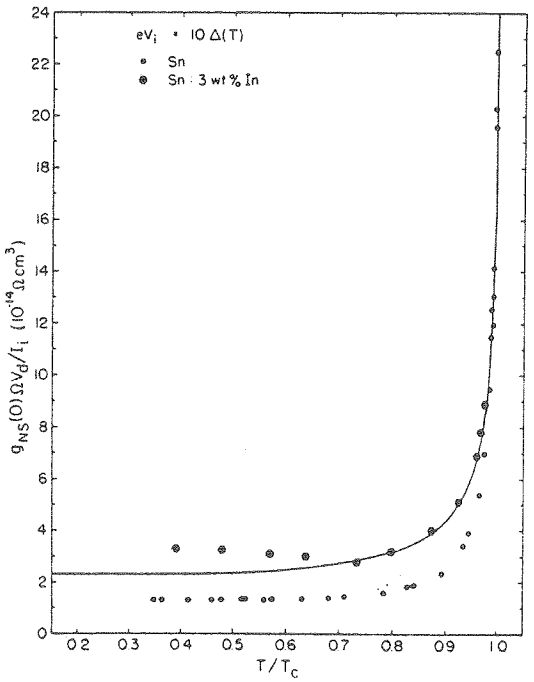

Fig. 12. $g_{NS}(0)\Omega V_d/I_i$ vs. T/T_c for pure Sn (•) and SnIn (◉). The solid line is a fit of $k_B T_c/\Delta(T)$ to the data for SnIn for $T/T_c \gtrsim 0.7$.

of samples of pure Sn, and for one set of samples of Sn with 3wt. %In. The mean free path in the clean Sn samples was always boundary limited, while that in the alloy was estimated to be 42nm. The fact that all the data for the clean Sn samples lie on a smooth curve demonstrates that the predicted dependence on volume is correct. Near T_c, for both clean and dirty samples V_d/I_i, which is proportional to $F^*\tau_{Q^*}$, diverges with increasing temperature. Below $T/T_c \approx 0.95$, the value of $F^*\tau_{Q^*}$ for the dirty sample is significantly larger than for the clean sample. We postpone a discussion of this difference to Sec. VA, and focus our attention on the behavior near T_c, where inelastic scattering makes the only significant contribution to charge relaxation.

The solid line is a fit to the data of the curve $g_{NS}(0)\Omega V_d/I_i = 4.0\times10^{-14}\ k_B T_c/\Delta(T)\ \Omega cm^3$ in the limit $T\to T_c$. Using the value* $N(0) = 1.39 \times 10^{22} eV^{-1} cm^{-3}$ in Eq. (2.25) we calculate $(F^*\tau_{Q^*})^{-1} = 5.6 \times 10^9\ (\Delta/k_B T_c)\ s^{-1}$. Equating this value with the prediction of Eq. (3.1), we find $\tau_E = 1.4 \times 10^{-10}$ s. By way of comparison, Kaplan et al. (1976) have computed $\tau_E = 2.6 \times 10^{-10}$ s using measured values of α^2F in a collision integral. We regard the agreement as satisfactory.

In the case of the Sn alloy, the fit of $(F^*\tau Q^*)^{-1}$ to the predicted temperature dependence is excellent down to $T/T_c \approx 0.7$, while the pure Sn data diverge from the prediction below $T/T_c \approx 0.98$. To understand the differences between the clean and dirty samples, we must investigate the effects of gap anisotropy on charge relaxation. This is the subject of Sec. VA.

V. CHARGE RELAXATION VIA ELASTIC SCATTERING PROCESSES

We now turn to a discussion of charge relaxation by elastic scattering, beginning with scattering from non-magnetic impurities in the presence of an anistropic energy gap. We then consider elastic scattering in the presence of a pair-breaking mechanism such as magnetic impurities or an applied supercurrent or magnetic field.

A. Elastic Scattering with an Anisotropic Energy Gap

We have already seen from Eq. (3.2) that the coherence factor

*This value was computed from $N(0) = 3\gamma/2\pi^2 k_B^2$, where γ is the coefficient of the electronic heat capacity taken from Kittel (1976).

$(uu'-vv')^2$ forbids charge relaxation via elastic scattering when the energy gap is isotropic. However, when the gap is anisotropic the coherence factor no longer vanishes, and elastic scattering can transfer quasiparticles between the $k_>$ and $k_<$ branches. Figure 13 shows the excitation spectra at two regions of the Fermi surface at which the energy gap is different. Since the values of $|\xi|$ and $|\xi'|$ are different for the initial and final states, the coherence factor is non-zero even though E and E' are identical. This situation was first discussed by Tinkham (1972), and subsequently, more quantitatively, by Chi and Clarke (1979). We shall follow the latter treatment.

The elastic scattering rate $G_{el\xi}$ that appears in the Boltzmann Equation [Eq. (3.4)] is given by

$$G_{el\xi} = \frac{\tau_1^{-1}}{2}\left\langle \rho_{\Delta'}(E)\left[1 - \frac{\Delta\Delta'}{E^2} - \left(1 - \frac{\Delta^2}{E^2}\right)^{\frac{1}{2}}\left(1 - \frac{\Delta'^2}{E^2}\right)^{\frac{1}{2}}\right]\right\rangle_{\Delta,\Delta'} \times$$

$$[f_\xi\,(1-f_{\xi'}) - f_{\xi'}(1-f_\xi)]. \qquad (5.1)$$

Here, τ_1^{-1} is the elastic scattering rate of an electron when the metal is in the normal state, $\rho_{\Delta'}(E)$ is the final density of states, one-half times the first square bracket is the coherence factor, and the two terms in the second square bracket are the occupation factors for elastic scattering from ξ to ξ' and the reverse process, respectively. The symbol $\langle\ \rangle_{\Delta,\Delta'}$ indicates an angular average over the gap-anisotropy distribution. To average the coherence factor we set $\Delta = \bar{\Delta} + \delta$ and $\Delta' = \bar{\Delta} + \delta'$, where $\bar{\Delta}$ is the average energy gap. Our goal is to express the terms in $\langle\ \rangle$ in terms of the mean square gap anisotropy

$$\langle\delta^2\rangle = \langle(\Delta-\bar{\Delta})^2\rangle. \qquad (5.2)$$

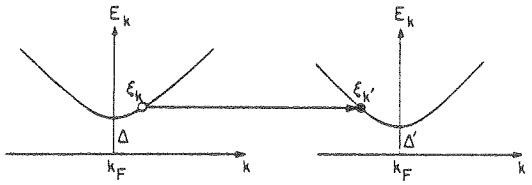

Fig. 13. Principle of charge relaxation by elastic scattering in the presence of gap anisotropy. The two excitation spectrum refer to two different regions of the Fermi surface where the energy gaps are different.

We first note that if one expands $\rho_{\Delta'}(E) = \rho_{\bar{\Delta}}(E)+(\partial\rho(E)/\partial\Delta')\delta\Delta'$, it can be shown that the second term is a higher order correction. Thus we set $\rho_{\Delta'}(E) = \rho_{\bar{\Delta}}(E) = E/(E^2-\bar{\Delta}^2)^{\frac{1}{2}}$. One substitutes for Δ and Δ' in the coherence factor, and expands with $E>>\bar{\Delta}$. Using the fact that $\langle\delta\rangle_{\Delta} = \langle\delta'\rangle_{\Delta'} = 0$, we find $\langle(uu'-vv')^2\rangle_{\Delta,\Delta'} = \langle\delta^2\rangle/2(E^2-\Delta^2)$. Clearly, this expression is meaningless for $E \leq \bar{\Delta}$. However, for the purpose of the present calculation it is an adequate approximation to use this expression for $E>\bar{\Delta} + \langle\delta^2\rangle^{\frac{1}{2}}/2$, and to take the value at $E = \bar{\Delta} + \langle\delta^2\rangle^{\frac{1}{2}}/2$ for lower energies; the error introduced is of the order of $\langle\delta^2\rangle^{\frac{1}{2}}/\bar{\Delta}$. Thus, we find

$$\langle\rho_{\Delta'}(E)\ (uu'-vv')^2\rangle_{\Delta,\Delta'} = \langle\delta^2\rangle\ E/2(E^2-\Delta^2)^{\frac{3}{2}}\quad (E\geq\bar{\Delta}+\langle\delta^2\rangle^{\frac{1}{2}}/2) \tag{5.3}$$

We define the normalized mean-square gap anisotropy (Markowitz and Kadanoff 1963) by

$$\langle a^2\rangle = \langle\delta^2\rangle/\bar{\Delta}^2\ . \tag{5.4}$$

For clean bulk superconductors ($\ell>>\hbar v_F/\Delta$), $\langle a^2\rangle$ is a constant, independent of temperature. However, if the mean free path is shortened by impurity or surface scattering, $\langle a^2\rangle$ is reduced from its clean limit value, $\langle a^2\rangle_o$ (Anderson 1959), to a value given approximately by

$$\langle a^2\rangle = \langle a^2\rangle_o/[1 + (\hbar/2\tau_1\bar{\Delta})^2]. \tag{5.5}$$

Combining Eqs. (5.1), (5.3), (5.4) and (5.5) for $E\geq\bar{\Delta}+\langle\delta^2\rangle^{\frac{1}{2}}/2$ we arrive at our final expression for $G_{el\xi}$:

$$G_{el\xi} = \tau_1^{-1}\ \frac{\langle a^2\rangle_o}{1+(\hbar/2\tau_1\bar{\Delta})^2}\ \frac{\bar{\Delta}^2E}{2(E^2-\bar{\Delta}^2)^{3/2}}\ (f_{\xi}-f_{-\xi}).\quad (E\geq\bar{\Delta}+\langle\delta^2\rangle^{\frac{1}{2}}/2) \tag{5.6}$$

In Eq. (5.6), we have set $\xi'=-\xi$; this is an excellent approximation for the values of anisotropy encountered in real metals.

It is instructive to consider $G_{el\xi}$ as a function of τ_1^{-1}. First, consider the clean limit in which $(\hbar/2\tau_1\bar{\Delta})^2<<1$, i.e. $\ell>>\hbar v_F/2\bar{\Delta}$. As we progressively increase τ_1^{-1}, for example, by adding impurities, $G_{el\xi}$ increases proportionately; in this limit, shortening the mean

free path increases the scattering rate much more than it decreases the mean square anisotropy. On the other hand, in the dirty limit $(\hbar/2\tau_1\bar{\Delta})^2 >> 1$, $G_{el\xi}$ is proportional to τ_1. Thus, as we increase τ_Q^{-1}, $G_{el\xi}$ decreases; in this limit the mean square anisotropy is reduced more rapidly than the scattering rate is increased. From Eq. (5.6) it is evident that at a given temperature the scattering rate is a maximum when $\tau_1^{-1} = \hbar/2\bar{\Delta}$ or $\ell = \hbar v_F/2\bar{\Delta}$. Thus, sufficiently close to T_c, the sample must be in the limit in which $\hbar/2\tau_1\bar{\Delta} >> 1$, and $G_{el\xi}$ will be proportional to $\tau_1\bar{\Delta}^4/(k_BT_c)^2$ for typical quasiparticle energies $\sim k_BT_c$. Thus, we expect the elastic charge relaxation rate to fall off very much more rapidly than the inelastic rate as $T \to T_c$, so that the inelastic rate eventually dominates above a temperature that depends on the relative magnitudes of τ_1^{-1} and τ_E^{-1}.

We are now in a position to understand qualitatively the behavior of the Sn and SnIn films in Fig. 12. For the clean Sn films, the mean free path is roughly the film thickness, say 300nm on the average. Consider first temperatures below about $0.8T_c$. In Table I we list values of τ_1^{-1}, $(\hbar/2\bar{\Delta}\tau_1)^2$ and $\tau_1^{-1}[1 + (\hbar/2\bar{\Delta}\tau_1)^2]^{-1}$ evaluated at low temperatures using $\bar{\Delta} = 1.76\ k_BT_c$, with $T_c = 3.8K$. We see that the elastic charge relaxation rate is expected to be

Table I. Parameters for the Sn and SnIn Films in Fig. 12[a].

	Sn	SnIn
ℓ(nm)	≈300	42
$\tau_1^{-1}(ps^{-1})$	2.2	15.5
$(\hbar/3.52k_BT_c\tau_1)^2$	1.60	79
$\tau_1^{-1}[1 + (\hbar/3.52k_BT_c\tau_1)^2]^{-1}(ps^{-1})$	0.85	0.19

a. We used $v_F = 0.65 \times 10^6 ms^{-1}$, calculated from $v_F = (\pi^2k_B^2/e^2\gamma)\sigma/\ell$ (Pippard 1965), where σ is the conductivity and $\sigma/\ell = 9.5 \times 10^{10}\Omega^{-1}cm^{-1}$ for Sn (Chambers 1952).

about 5 times faster in Sn than in SnIn. Since the total measured rate for both inelastic and elastic scattering is roughly two times higher in Sn than in SnIn, we conclude that the elastic contribution is relatively negligible for SnIn, but comparable with the inelastic rate for Sn. Now let us increase the temperature from $0.8T_c$. In the SnIn, the elastic charge relaxation rate becomes even more negligible compared with the inelastic rate. In the Sn, the elastic charge relaxation rate becomes progressively smaller than the inelastic rate, eventually becoming negligible when $\bar{\Delta}$ falls below a certain value. Thus, in the limit $T \to T_c$, the charge relaxation is due to inelastic scattering only, and the data for the Sn and SnIn samples merge together. Thus, sufficiently close to T_c, we are justified in using the data to extract values of T_E, as we did in Sec. IV.

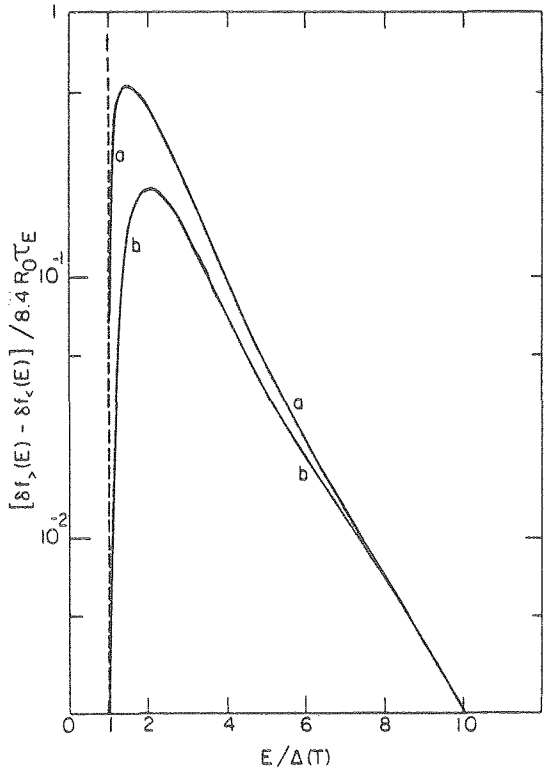

Fig. 14. Computed distribution for a 100nm-thick film at $0.9T_c$ with Δ=100meV for electrons injected from a normal film through a 1Ω 3x3mm tunnel junction biased at $10\Delta/e$. Curves a and b are for $\tau_{Q^*el}^{-1}(0)\tau_E$=0 and 0.93, respectively.

To account quantitatively for the charge relaxation by elastic scattering one must insert $G_{el\xi}$ into the Boltzmann equation, Eq. (3.4), and solve the equation numerically, retaining the injection and inelastic collision terms in their previous forms. This was undertaken by CC, who calculated curves appropriate for their results on Al films. These films were always in the limit $(\hbar/2\bar{\Delta}\tau_1)^2 >> 1$ so that we can write Eq. (5.6) in the form

$$G_{el\xi} = \tau_{Q^*el}^{-1}(0)\left(\frac{\bar{\Delta}}{k_B T_c}\right)^2 \frac{E\bar{\Delta}^2}{(E^2-\bar{\Delta})^{3/2}}(f_\xi - f_{-\xi}), \quad [(\hbar/2\bar{\Delta}\tau_1)^2 >> 1)] \tag{5.7}$$

where

$$\tau_{Q^*el}^{-1}(0) = 2\tau_1(k_B T_c)^2 \langle a^2 \rangle_o / \hbar^2 \tag{5.8}$$

is a characteristic elastic charge relaxation rate. Figure 14 shows the results of CC for $\tau_{Q^*el}^{-1}(0)\tau_E = 0$, and $\tau_{Q^*el}^{-1}(0)\tau_E = 0.93$. We see that the addition of the elastic relaxation process reduces the charge imbalance, and shifts the peak in the distribution to higher energies. This shift illustrates the fact that the elastic relaxation is much faster at low energies than at high energies,

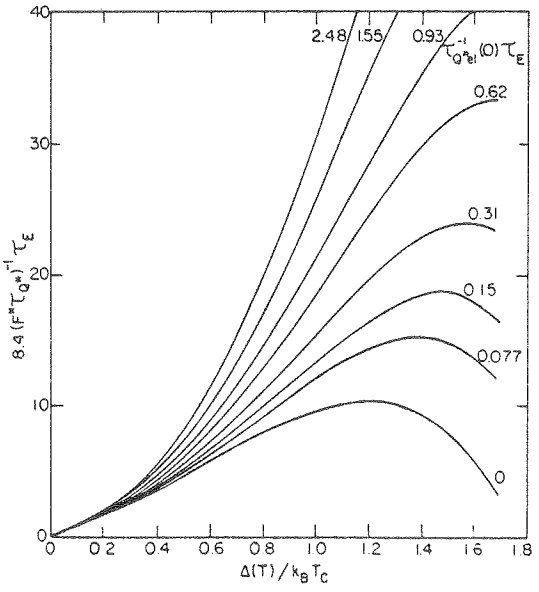

Fig. 15. Calculated values of $(F^*\tau_{Q^*}/8.4\tau_E)^{-1}$ vs. $\Delta(T)/k_B T_c$ for 8 values of $\tau_{Q^*el}^{-1}(0)\tau_E$ with $V_i = 10\Delta(T)/e$.

because of the term $(E^2-\Delta^2)^{-3/2}$ in Eq. (5.7). Figure 15 shows the computed curves of $(F^*\tau_{Q^*}/\tau_E)^{-1}$ vs. $\Delta(T)/k_BT_c$ for 8 values of $\tau^{-1}_{Q^*el}(0)\tau_E$. As $\Delta/k_BT_c \to 0$, the elastic rate becomes negligible, and all the curves tend to the same limit, which is just the inelastic charge relaxation rate. At lower temperatures, the charge relaxation rates increase monotonically with $\tau^{-1}_{Q^*el}(0)\tau_E$, as one would expect.

The sample configuration used by CC for the experiments was similar to that in Fig. 1, and is shown in the inset of Fig. 16. The injector film was in the superconducting state for most of the measurements. The mean free path of some of the samples was reduced, and, at the same time, the transition temperature increased by evaporating the Al in a partial pressure of oxygen. The transition temperatures and mean free paths of the cleanest and dirtiest samples were 1.22K and 409nm and 2.11K and 1nm, respectively. Since the detector junction resistances were relatively large ($\sim$1mΩ), and the values of V_d were also quite large because of the

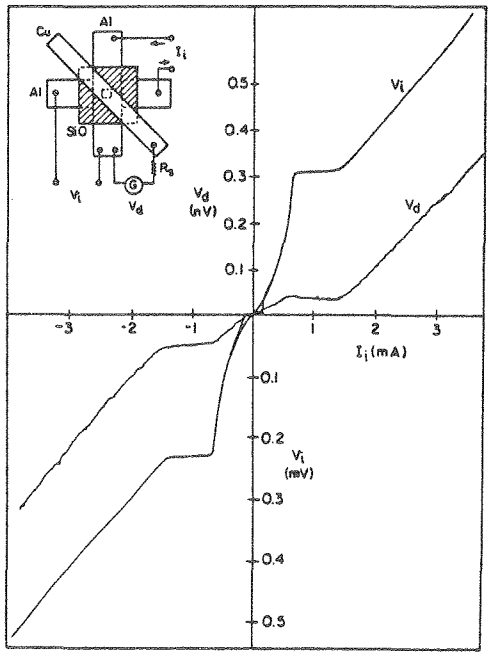

Fig. 16. Measured V_i and V_d vs. I_i for a representative sample at T/T_c=0.87. Note the two different voltage scales. Inset shows sample configuration.

long electron-phonon scattering time in Al, it was not necessary to deposit a Pb film over the Cu to reduce the series resistance. Consequently, pure Cu was used to complete the detector junction.

Figure 16 shows plots of V_i and V_d vs. I_i for a representative sample. It is noteworthy that when I_i increases at the sum of the gaps of the injector and injected films (approximately 0.23mV), V_d remains essentially constant. This is because additional electrons injected by the current increase have an energy Δ, and equally populate the $k_>$ and $k_<$ branches, thereby creating zero charge imbalance. This result is a direct proof that V_d is proportional to Q*.

The dots in Fig. 17 show $(F^*\tau_{Q^*})^{-1}$ vs. $\Delta(T)/k_BT_c$ for 5 representative samples with parameters listed in Table II; N(0) =

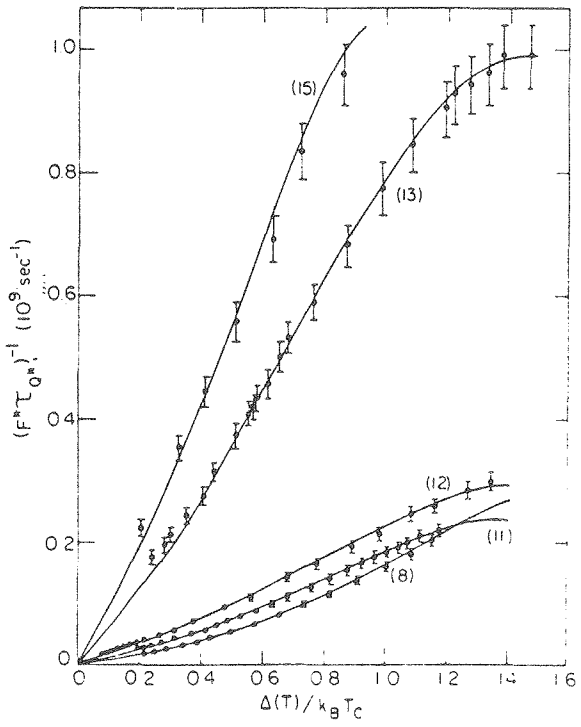

Fig. 17. Measured values (•) of $(F^*\tau_{Q^*})^{-1}$ vs. Δ/k_BT_c for 5 samples listed in Table II (sample numbers shown in parenthesis). The solid lines are a best fit to the solution of the Boltzmann equation.

Table II. Measured and Calculated Quantities for Five Al Samples[a]

Sample	T_c(K)	ℓ(nm)	τ_E(ns)	$\tau_{Q^*el}^{-1}(0)\tau_E$	$\langle a^2 \rangle_o$
8	1.267	78	13	0.62	0.022
11	1.306	23	8	0.093	0.017
12	1.411	12.5	5.8	0.062	0.025
13	1.573	6.0	1.5	0.031	0.076
15	2.113	1.0	1.0	b	b

a. We used $v_F = 1.36 \times 10^6 ms^{-1}$, calculated from the free electron value divided by the thermal effective electron mass (Kittel 1976), $\rho\ell = 9 \times 10^{-16} \Omega m^2$ (Fickett 1971), and $N(0) = 1.74 \times 10^{28} eV^{-1} m^{-3}$ (Gschneider 1964).

b. The upward curvature was too small to enable an estimate of $\tau_{Q^*el}^{-1}(0)$ to be made.

1.74×10^{28} $eV^{-1}m^{-3}$ (Gschneider 1964). The solid lines are the best fits to the computed solution of the Boltzmann equation using the fitting parameters τ_E^{-1} and $\tau_{Q^*el}^{-1}(0)\tau_E$ shown in Table II. The fit to the data (and to the data of the 10 other samples measured) is excellent. For each sample we determined τ_E^{-1} from the slope in the limit $\Delta(T)/k_BT_c \to 0$, while we found $\tau_{Q^*el}^{-1}(0)\tau_E$ from the upward curvature needed to fit the data at lower temperatures. The values of $\langle a^2 \rangle_o$ deduced from these data were usually 2 or more times larger than the value of 0.01 reported elsewhere (Leavens and Carbotte 1971, 1972, Blackford 1976). However, it should be realized that the values of $\langle a^2 \rangle$ in these thin Al films are very small: For the cleanest film measured, with ℓ=317nm, $\langle a^2 \rangle \approx 2 \times 10^{-4} \langle a^2 \rangle_o$ at $0.9T_c$. The remarkable sensitivity of $\tau_{Q^*}^{-1}$ to small gap anisotropies reflects the weak electron-phonon interaction in Al. A similar degree of anisotropy in Sn would not have an observable effect on $\tau_{Q^*}^{-1}$.

For the cleanest Al films studied (not listed in Table II) the average value of τ_E was about 12ns. This value is in good agreement with that obtained from measurements of the 2Δ-phonon mean free path (Long 1973) and of gap relaxation (Schuller and Gray 1977), but about a factor of 4 shorter than the values obtained from recombination time measurements (Gray et al. 1969, Smith and Mochel 1976, Chi and Langenberg 1976) and from theoretical estimates (Kaplan et al. 1976, Lawrence and Meador 1978). The fact that the values of τ_E seem to fall into two groups, one clustered around 12ns and the other around 48ns is most peculiar, and at present remains an unsolved mystery. The dependence of τ_E^{-1} on T_c was also unexpected: One would expect τ_E^{-1} to be proportional to T_c^3 (Kaplan et al. 1976), but a much stronger dependence was observed, perhaps T_c^5. This observation could possibly be explained by an increase in $\alpha^2F(\omega)$ with increasing disorder (Bergmann 1971, Zavaritski 1969, Knorr and Barth 1970). Another suggestion made by CC is that oxygen atoms on the surface and/or at grain boundaries have dangling bands with magnetic moments due to the localized unpaired electrons. These magnetic moments could increase the charge relaxation rate through elastic spin-flip scattering (see Sec. VB). Since the density of magnetic moments is proportional to the oxygen doping level, and increases with T_c, this mechanism could explain the apparent rapid increase of τ_E^{-1} with T_c. In fact, in a quantitative analysis, CC

showed that this hypothesis was consistent with the observations. At present, this matter remains unresolved. However, despite the questions remaining over the values of τ_E^{-1} and its dependence on T_c, the theory accounts satisfactority for the relaxations of Q* by elastic scattering in the presence of gap anisotropy.

B. Elastic Scattering from Magnetic Impurities

The addition of magnetic impurities to a superconductor destroys the degeneracy between time-reversed electron states through the exchange interaction between the conduction electrons and the impurities, and thereby gives the Cooper pairs a finite lifetime, the inverse of which is called the pair-breaking rate (Abrikosov and Gor'kov 1960). The pair breaking rate is the elastic spin-flip scattering rate, τ_S^{-1}, for electrons in the normal metal. A small concentration of impurities also smears out the peak in the BCS density of states over an energy range $\hbar/\tau_S$ (so that the energy gap and the order parameters are no longer equal), depresses the transition temperature by $\pi\hbar/4k_B\tau_S$, and alters the temperature dependence of the order parameter from the usual BCS form. In addition, the impurities can have a dramatic effect on the charge relaxation rate, as was first pointed out by Schmid and Schön (SS, 1975) and later studied by Pethick and Smith (1980), Entin-Wohlman and Orbach (1979), and Lemberger and Clarke (LC 1980). The essential reason can be understood by realizing that the coherence factor for elastic spin-flip scattering from one quasiparticle branch to the other is in an isotropic superconductor is not zero, but of the form

$$(uu'+vv')^2 = 4u^2v^2 = \Delta^2/E^2. \tag{5.9}$$

Since this factor approaches unity as $E\to\Delta$, we expect the spin-flip scattering to have an appreciable effect on $\tau_{Q^*}^{-1}$ when $\tau_S^{-1} \gtrsim \tau_E^{-1}$.

SS found

$$(F^*\tau_{Q^*})^{-1} = \frac{\pi\Delta}{4k_BT_c\tau_E}\left(1+\frac{2\tau_E}{\tau_S}\right)^{\frac{1}{2}}. \quad (\tau_{Q^*}^{-1}<<\tau_E^{-1}) \tag{5.10}$$

A factor $(1+\hbar^2\Gamma/\Delta^2\tau_E)^{\frac{1}{2}}$ has been omitted in Eq. (5.10), where $\Gamma=(2\tau_E)^{-1}+\tau_s^{-1}$, since it is very close to unity for all values of τ_E, τ_S, and Δ used in the experiments to be described later. This factor accounts for the effect of the smearing in the density of

states on $\tau_{Q^*}^{-1}$. We will now interpret Eq. (5.10) physically. First, consider the limit $\tau_S^{-1} \ll \tau_E^{-1}$ in which the spin-flip scattering is a weak perturbation on the inelastic scattering, and to a first approximation does not affect the quasiparticle distribution created by the inelastic processes. Equation (5.10) can be expanded to give

$$\frac{1}{F^*\tau_{Q^*}} = \frac{\pi\Delta}{4k_BT_c}\left(\frac{1}{\tau_E} + \frac{1}{\tau_S}\right). \quad (\tau_S^{-1} \ll \tau_E^{-1},\ \tau_{Q^*}^{-1} \ll \tau_E^{-1}) \tag{5.11}$$

The spin-flip term, $\pi\Delta/4k_BT_c\tau_S$, has this form because the coherence factor is substantial only for quasiparticles in the range from Δ to $\sim 2\Delta$, so that only a fraction $\sim\Delta/k_BT_c$ of the excess quasiparticles can relax through this channel.

In the limit $\tau_S^{-1} \gg \tau_E^{-1}$, Eq. (5.10) reduces to

$$\frac{1}{F^*\tau_{Q^*}} = \frac{\pi\Delta}{4k_BT_c}\left(\frac{2}{\tau_E\tau_S}\right)^{\frac{1}{2}}. \quad (\tau_S^{-1} \gg \tau_E^{-1},\ \tau_{Q^*}^{-1} \ll \tau_E^{-1}) \tag{5.12}$$

In this limit, the spin-flip scattering modifies the quasiparticle distribution substantially because the lower energy excess quasiparticles undergo spin-flip scattering to the other branch more rapidly than higher energy quasiparticles can cool to replace them. As a result, the energy below which spin-flip charge relaxation is important is increased from $\sim 2\Delta$ to an energy E^*. We estimate this energy by equating the cooling rate, $\sim\tau_E^{-1}$, with the spin-flip branch crossing rate, $\sim\Delta^2/E^{*2}\tau_S$, to find $E^* \sim \Delta(\tau_E/\tau_S)^{\frac{1}{2}} \gg \Delta$. Thus, at temperatures near T_c, of the quasiparticles scattered downwards by the cooling process, a fraction $\sim E^*/k_BT_c$ contributes significantly to charge relaxation, so that the rate is $\sim E^*/k_BT_c\tau_E \sim (\Delta/k_BT_c)(\tau_E\tau_S)^{-\frac{1}{2}}$, in essential agreement with Eq. (5.12). We emphasize that τ_E^{-1} enters the result not because it contributes to the charge relaxation <u>per se</u>, but because it determines the rate at which quasiparticles scatter downwards into the region from which they spin-flip scatter to the other branch.

LC extended CC's computer solution of the Boltzmann equation to include the spin-flip term. The purpose of this investigation was both to check the validity of Eq. (5.10) and to extend the theory to lower temperatures. The spin-flip scattering rate for a quasiparticle at energy ξ is

$$G_{sf\xi} = \frac{1}{\tau_S} \frac{\Delta^2}{E^2} \frac{E}{|\xi|} (f_\xi - f_{-\xi}). \qquad (5.13)$$

The term τ_S^{-1} is just the elastic spin-flip scattering rate, Δ^2/E^2 is the coherence factor [Eq. (5.9)], $E/|\xi|$ is the final density of states, and $(f_\xi - f_{-\xi})$ is the usual occupation factor. LC added this term to the Boltzmann equation, Eq. (3.4), deleted the term $G_{el\xi}$, since this is negligible compared with $G_{sf\xi}$ for magnetic impurity concentrations of experimental interest, and solved the equation on a computer. Figure 18 shows the distribution for several values of τ_E/τ_S. As expected $(\delta f_\xi - \delta f_{-\xi})$ decreases at all energies as τ_E/τ_S increases. Furthermore, $(\delta f_\xi - \delta f_{-\xi})$ decreases more at low energies than at high energies, and the peak therefore moves to higher

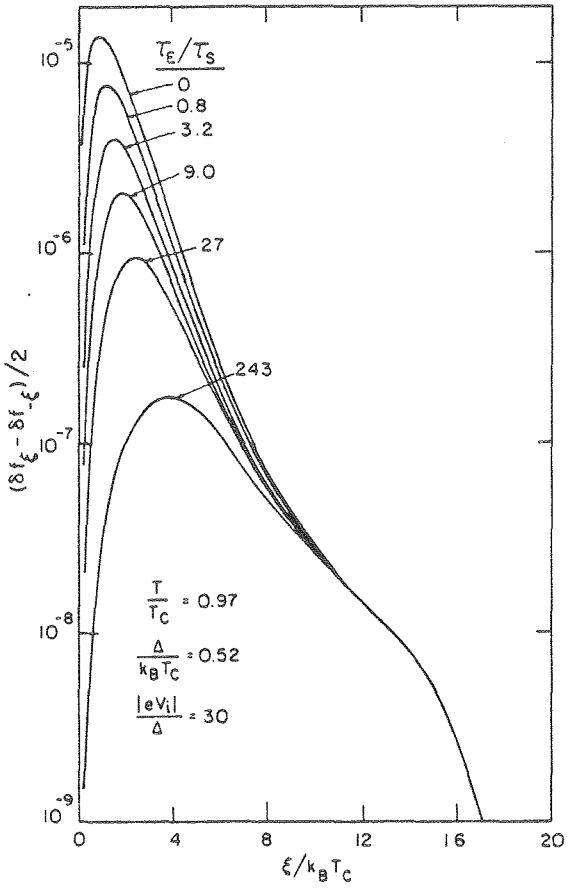

Fig. 18. $(\delta f_\xi - \delta f_{-\xi})/2$ vs. E/Δ for several values of τ_E/τ_S with $R_o = 200 s^{-1}$ and $\tau_E^{-1} = 10^8 s^{-1}$.

energies, because the spin-flip collision operator [Eq. (5.3)] is proportional to $\Delta^2/E|\xi|$. This is a graphic demonstration of the picture in which the low-lying excitations are rapidly relaxed by spin-flip scattering, thus depleting the charge-imbalance at low energies because of the relatively slow rate at which high energy injected quasiparticles can be cooled into this energy range by phonon scattering.

Figure 19 shows $(F^*\tau_{Q^*})^{-1}$, normalized to the SS factor $(\pi/4\tau_E)(1 + 2\tau_E/\tau_S)^{\frac{1}{2}}$ vs. Δ/k_BT_c for several values of τ_E/τ_S. For $\Delta/k_BT<1$ the computed values of $(F^*\tau_{Q^*})^{-1}$ lie above the SS result (except at $\Delta/k_BT_c=0$), by an amount that increases with τ_E/τ_S. This discrepancy persists to $\tau_E/\tau_S=0$, as is also shown in Fig. 8. Furthermore, for all values of Δ/k_BT_c, the calculated values of $[(\pi F^*\tau_{Q^*}/4\tau_E)(1 + 2\tau_E/\tau_S)^{\frac{1}{2}}]^{-1}$ increase monotonically with τ_E/τ_S.

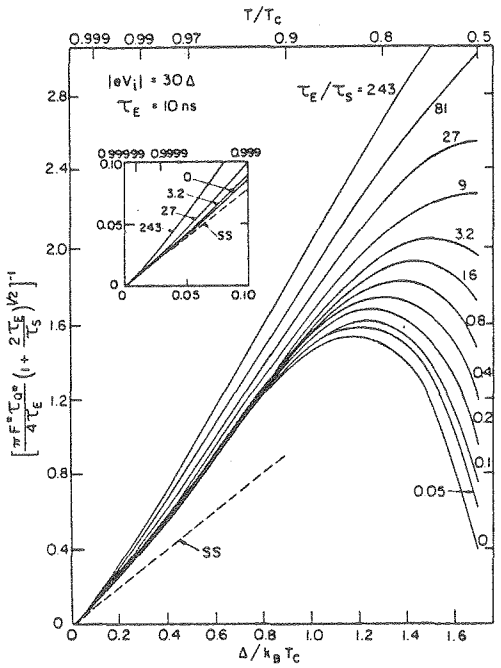

Fig. 19. $(F^*\tau_{Q^*})^{-1}$ normalized to $(\pi/4\tau_E)(1 + 2\tau_E/\tau_S)^{1/2}$ vs. Δ/k_BT_c. The curves approach the origin with unity slope. The dashed line is an extrapolation of the SS theory to low temperatures. The inset shows the region near the origin.

LC measured τ_{Q*}^{-1} in Al films doped with Er, a magnetic impurity. The samples had the configuration shown in Fig. 16, except in that the edges of both junctions were masked with SiO. The AlEr films were deposited by evaporating small pellets to completion. Figure 20 is a plot of $(F^*\tau_{Q*})^{-1}$ (obtained for $V_i >> \Delta/e$) vs. Δ/k_BT_c for three samples with different impurity concentrations. The relevant parameters are listed in Table III, with $\tau_E = 12\text{ns}(1.2/T_c)^3$ [Clarke and Chi 1979, Eq. (1.11)], and the spin-flip rate estimated from the data of Craven et al. (1971), $\tau_S^{-1} = (1.9\pm0.4) \times 10^{13} n_{Er} s^{-1}$, where n_{Er} is the concentration of Er atoms. For each sample plotted, $(F^*\tau_{Q*})^{-1}$ is linear in Δ/k_BT_c up to a value of about 0.8 ($T \approx 0.92T_c$), tending to flatten off as Δ/k_BT_c increases further. The initial linear behavior is consistent with the SS result Eq. (5.10) provided one extrapolates the SS result to substantially higher values of of Δ/k_BT_c than is justified a priori. The linear regions were used

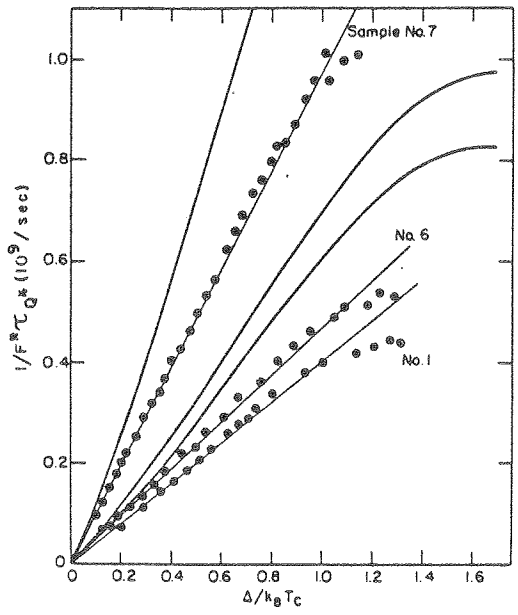

Fig. 20. Experimental values of $(F^*\tau_{Q*})^{-1}$ vs. Δ/k_BT_c for samples with Er concentrations of 21(#1), 81(#6), and 220(#7) at. ppm, with straight lines drawn through the data by eye. The other curves, which represent computer solutions to the Boltzmann equation, have the same slope as the data in the limit $\Delta/k_BT_c \to 0$.

Table III. Measured and Calculated Parameters for AlEr Films[a]

Sample	Er conc (ppm)	T_c (K)	ℓ (nm)	τ_E (ns)	τ_S(est.) (ps)	τ_S(meas.) (ps)
1	21	1.338	38	8.6	2500	1100
6	81	1.350	32	8.3	650	860
7	220	1.410	22	7.4	240	210

a. ℓ is obtained from $\rho\ell = 9 \times 10^{-16} \Omega m^2$ (Fickett 1971), and $N(0) = 1.74 \times 10^{28} eV^{-1} m^{-3}$ (Gschneider 1964). The value of τ_S(est.) is taken from Craven et al. (1971).

to obtain the values of τ_S (measured) listed in Table III. These values are all within a factor of 2 or better of the estimated values. As a further test of the applicability of the SS theory, in Fig. 21 we plot the measured values of the slope S of the linear region for all samples vs. the SS expression $(\pi/4\tau_E)(1 + 2\tau_E/\tau_S)^{\frac{1}{2}}$, using the values of τ_E and τ_S (estimated) from Table III. The general agreement is good, implying that the SS result accurately describes the observed dependence of $1/F^*\tau_{Q^*}$ on Δ/k_BT_c, and τ_E/τ_S for $\Delta/k_BT_c \lesssim 0.8$.

Figure 20 also shows curves computed from the Boltzmann equation using the values at τ_E and τ_S (measured) from Table III. It is immediately clear that, rather than providing a better fit to the data than the extrapolated SS result, the computed curves give a much worse fit. LS tried various other fitting procedures, but were not able to produce an acceptable fit. The discrepancy between the computed and experimental curves is further emphasized in Fig. 22, where $(SF^*\tau_{Q^*})^{-1}$ is plotted vs. Δ/k_BT_c for one sample of each Er concentration. Although there is a spread in the results for the larger values of Δ/k_BT_c, it is apparent that the data, normalized in this way, lie on a universal curve. This is in complete contrast to the computed curves shown in Fig. 19, in which the same quantity increases markedly with τ_E/τ_S at a given temperature.

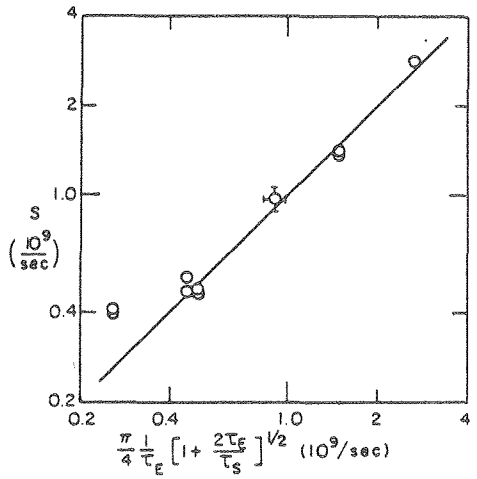

Fig. 21. S (slope of $(F^*\tau_{Q^*})^{-1}$ vs. Δ/k_BT_c for small Δ/k_BT_c) vs. $(\pi/4\tau_E)(1 + 2\tau_E/\tau_S)^{1/2}$ for all samples. The solid line through the origin has unity slope.

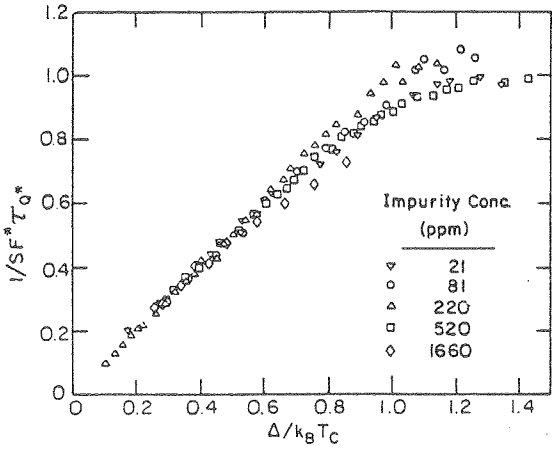

Fig. 22. $(SF^*\tau_{Q^*})^{-1}$ vs. Δ/k_BT_c for one representative sample of each impurity concentration.

This marked discrepancy between the data and the computed curves is extremely puzzling. It cannot be explained by invoking an additional charge-relaxation mechanism in the experiments, for example, Andreév (1964) reflection at a non-uniform gap or at the surface of the film, because the experimental rate $(F^*\tau_{Q^*})^{-1}$ lies substantially below, rather than above the computed rate. One can also rule out the possibility of impurity-impurity interactions, and of Kondo anomalies. It appears that either the collision operator for spin-flip scattering, Eq. (5.13), is inappropriate for charge relaxation or that the Boltzmann equation is not an adequate description of charge relaxation in the presence of magnetic impurities. On the other hand, the Schmid-Schön result, Eq. (5.10), provides a very satisfactory fit to the data over a much wider temperature range than can reasonably be expected.

C. Elastic Scattering in the Presence of a Supercurrent

When a supercurrent flows in a superconductor, the quasiparticle energies are raised by an amount $\vec{p}_k \cdot \vec{v}_s$, where $\vec{p}_k$ is the momentum of a quasiparticle in state $\vec{k}$, and $\vec{v}_s$ is the superfluid velocity (Aronov 1974, Galperin et al. 1974). Thus, quasiparticles at the Fermi energy where $\vec{v}_s$ and $\vec{p}_k$ are in the same direction are raised by $p_F v_s$, while those where $\vec{v}_s$ and $\vec{p}_k$ are in opposite directions are lowered by $p_F v_s$. This current-induced anisotropy allows elastic scattering between $\vec{k}_<$ and $\vec{k}_>$ states in much the same way as an in-

trinsic gap anisotropy (Fig. 13). Maki (1969) has shown that an appropriate electron relaxation rate for thin films [$d<<(\ell\xi_o)^{\frac{1}{2}}$] in the dirty limit ($\ell<<\xi_o$) is

$$\frac{1}{\tau_S} = \frac{\ell v_F}{6}\left(\frac{p_S}{\hbar}\right)^2 , \tag{5.14}$$

where d is the film thickness, $\xi_o = \hbar v_F/\pi\Delta(0)$, and $\vec{p}_S$ is the momentum of a Cooper pair. We can use Eq. (5.14) in Eq. (5.10) or (5.13) to predict the charge relaxation rate as a function of p_S. For the case of magnetic impurities LC found that at a given temperature $(F^*\tau_{Q^*})^{-1}$ was proportional to $(1 + 2\tau_E/\tau_S)^{\frac{1}{2}}$, as predicted by SS. Thus, we can immediately write down an expression for the detector voltage at a given temperature and injection current in the presence of a supercurrrent, I_S:

$$V_d(I_S) = \frac{V_d(0)}{(1 + 2\tau_E/\tau_S)^{\frac{1}{2}}} = \frac{V_d(0)}{(1 + b^{SS}I_S^{\,2})^{\frac{1}{2}}} , \tag{5.15}$$

where from Eq. (5.14),

$$b^{SS} = 2\tau_E/\tau_S I_S^{\,2} = \tau_E \ell v_F p_S^{\,2}/3\hbar^2 I_S^{\,2}. \tag{5.16}$$

For uniform currents much less than the critical current we can use the relations (Tinkham 1975) $\vec{p}_S = 2m\vec{v}_S$, $\vec{j}_{S_{\frac{1}{2}}} = n_S e v_S$, $n_S = mc^2/4\pi e^2\lambda^2$ and, in the dirty limit, $\lambda(0) \approx \lambda_L(0)(\xi_o/\ell)^{\frac{1}{2}}$ to find

$$b^{SS} = \left(\frac{8\pi e}{\hbar c^2}\right)^2 \frac{\tau_E v_F \xi_o^{\,2}\lambda_L^4(0)}{3\ell d^2 w^2} \frac{\lambda^4(T/T_c)}{\lambda^4(0)} . \tag{5.17}$$

Here, w is the film width, $\lambda_L(0)$ is the London penetration depth, and $\lambda(T/T_c)/\lambda(0)$ is a well-known function (Tinkham 1975). Equations (5.15) and (5.17) thus represent the SS prediction for the effect of a supercurrent on the value of Q* at fixed temperature and injection current.

Lemberger and Clarke (1980a) solved the Boltzmann equation in the presence of a supercurrent by replacing $1/\tau_S$ in Eq. (5.13) with Eq. (5.14) to obtain

$$G_{S\xi} = \frac{\ell v_F}{6}\left(\frac{p_S}{\hbar}\right)^2 \frac{\Delta^2}{E|\xi|}\,(f_\xi - f_{-\xi}). \tag{5.18}$$

With this substitution, all of the results computed in Sec. VB can be carried over to the present case. Thus, for fixed temperature and injection voltage,

$$V_d(I_S) = \frac{V_d(0)}{(1 + b^{num} I_S^{\,2})^{1/2}}, \tag{5.19}$$

where $b^{num}(T)$ is the numerical value produced by the computer. In general, $b^{num}(T)$ will differ from $b^{SS}(T)$, as is evident in Sec. VB, and we can compare both values with the measured value, $b^{meas}(T)$.

Lemberger and Clarke (1980a) performed experiments using the usual geometry with a supercurrent introduced along the Al film in which the charge imbalance is generated. To increase the uniformity of the current distribution, a Nb groundplane was sputtered onto the substrate and covered with an insulating layer before the sample was deposited. A representative plot of $V_d(I_S)$ vs. I_S is shown in Fig. 23. As predicted by Eqs. (5.15) or (5.19), the value of $|V_d|$ decreased quadratically with increasing $|I_S|$ at low supercurrents, becoming linear in I_S at higher supercurrents. The slight asymmetry in the curves about $I_S=0$ was due to the non-negligible value of I_i. After shifting the origin appropriately, curves of the form $(1 + bI_S^{\,2})^{1/2}$ were fitted; the quality of the fit is excellent. Experimentally determined values of b are shown in Fig. 24 for two samples with parameters listed in Table IV. The fitted curves b^{SS} and b^{num} are also shown. The temperature dependence of b^{SS} is in excellent agreement with the data, while b^{num} is in substantial disagreement. Furthermore, the ratio $\langle b^{SS}(T)/b^{meas}(T)\rangle$ varies between $\frac{1}{3}$ and $\frac{1}{2}$, an agreement which, given the uncertainties in the values of v_F, ℓ, $\lambda_L(0)$, and τ_E, is considered to be quite acceptable.

We therefore draw the same conclusions as for the case of magnetic impurities: The Schmid-Schön theory fits the measured data very accurately, even at values of Δ/k_BT_c much larger than one could reasonably expect, while the computed solution to the Boltzmann equation does not fit the data. Thus, the problems with the Boltzmann equation approach to charge relaxation appear to apply to pair breaking mechanisms in general.

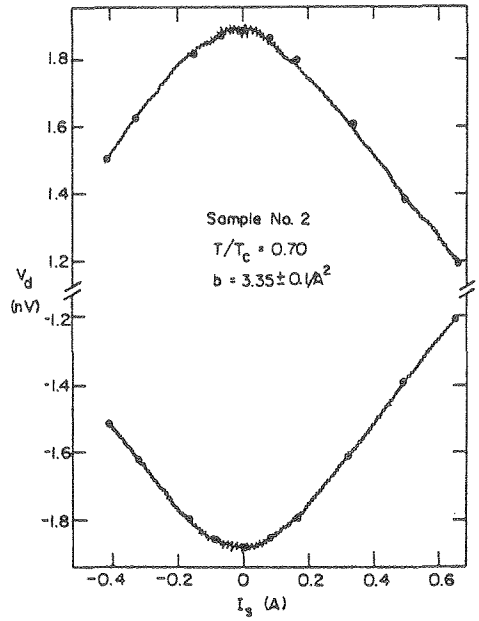

Fig. 23. Typical experimental plot of V_d vs. I_s for fixed I_i. The points are a fit to a function of the form $V_d(I_s) = V_d(0)/(1 + b\ I_s^2)^{1/2}$, with b as the fitting parameter.

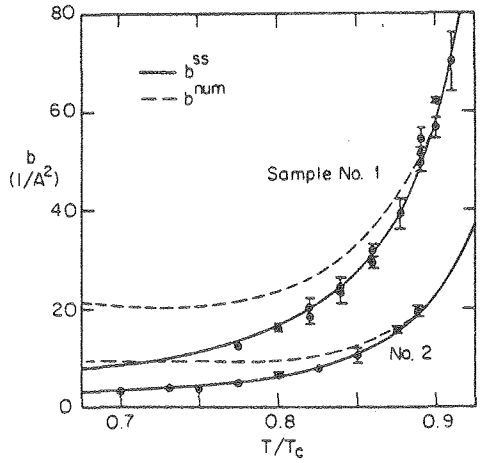

Fig. 24. Data points are measured values of b, solid and dashed lines are fits of b^{SS} and b^{num} to the data.

Table IV. Measured and Calculated Parameters for Samples 1 and 2[a]

Sample	T_c (K)	$\frac{R_{300}}{R_{4.2}}$	$\rho_{4.2}$ (nΩm)	ℓ (nm)	τ_E (ns)	$\left\langle \frac{b^{SS}}{b^{meas}} \right\rangle$
1	1.370	1.89	35.6	25	5.3	0.36
2	1.514	1.43	81.3	11	2.7	0.51

a. $R_{300}/R_{4.2}$ is the residual resistivity, $\rho_{4.2}$ is the resistivity of the Al film at 4.2K, ℓ is obtained from $\rho_{4.2}\ell = 9\times10^{-16}\ \Omega m^2$ (Fickett 1971). The values $N(0) = 1.74\times10^{28}\ eV^{-1}m^{-3}$ (Gschneidner 1964), $v_F = 1.36 \times 10^6\ ms^{-1}$ (Kittel 1976), and $\lambda_L(0) = 160$ nm (Meservey and Schwartz 1969) were used.

D. Elastic Scattering in the Presence of a Magnetic Field

An applied magnetic field is also a pair-breaking mechanism, and therefore creates a relaxation rate τ_S^{-1}. The exact form of this rate depends, for example, on whether the superconductor is a bulk sample or a thin film, and, in the latter case, whether the field is parallel or perpendicular to the plane of the film. Tinkham (1975) has given a useful summary of the results for τ_S^{-1}. The first demonstration of the essential correctness of the SS result Eq. (5.10), in the presence of a pair-breaking mechanism was by Kadin et al. in their study of phase slip centers. Subsequently, Hsiang (1980) measured the resistance of the SN interface in the presence of an applied magnetic field, and also found reasonable agreement with Eq. (5.10). For convenience, we will defer our discussion of these two experiments to Sec. VI.

VI. OTHER CHARGE IMBALANCE PHENOMENA

The final series of topics I am going to discuss concerns situations in which charge imbalance is generated by processes other than tunnel injection: The resistance of the normal metal-superconductor interface, phase slip centers, and the flow of a supercurrent in the presence of a temperature gradient.

A. The Resistance of the Normal Metal-Superconductor Interface

Pippard et al. (1971) measured the electrical resistance of superconductor-normal-metal-superconductor (SNS) sandwiches in which the normal metal was too thick and/or too dirty to sustain a Josephson supercurrent. They observed that, near the transition temperature of the superconductor, T_c, the resistance increased rapidly with increasing temperature. They ascribed this rise to the penetration of quasiparticles with energies greater than $\Delta_\infty(T)$ into the superconductor, where $\Delta_\infty(T)$ is the energy gap in S far from the interface. They also proposed that the additional boundary resistance was associated with a discontinuous jump in the electric potential at the NS interface, the electric field being zero throughout the superconductor. However, Yu and Mercereau (1972) showed that the potential did not fall abruptly to zero at the interface, but rather decayed exponentially in the superconductor. Subsequently, Harding et al. (1974) studied the resistance of SNS sandwiches in which the mean free path of the superconductor was shortened by alloying, and found an additional boundary resistance at low temperatures as well as a greatly enhanced rise in resistance near T_c.

The theory of the NS interface resistance has been widely investigated. The work of Rieger et al. (1971), who used a time-dependent Ginzburg-Landau theory, contained some essentially correct ideas, but did not produce the correct quasiparticle propagation length in the superconductor. Pippard et al. (1971) and Harding et al. (1974) used a Boltzmann equation approach that was later extended by Waldram (1975). The microscopic theory was developed by Schmid and Schön (1975), and has been extended by Ovchinnikov (1977, 1978), Artemenko and co-workers (1977, 1978) and Krähenbühl and Watts-Tobin (1978, 1979). Most recently, Hsiang and Clarke (1980) gave a simple description by adapting the tunnel injection theory that accounted quantitatively for their experimental data. In chapter 12, Pippard describes the Boltzmann equation approach for both the clean and dirty limits of the superconductor. I will confine myself to the clean limit ($\ell >> \xi(T)$), and follow closely the work of Hsiang and Clarke (HC).

When a charge imbalance is created in one region of a superconductor, it relaxes over a length

$$\lambda_{Q*} = (\ell v_F \tau_{Q*}/3)^{\frac{1}{2}}, \qquad (6.1)$$

where we assume $\ell << v_F \tau_{Q*}$. Very close to T_c ($\Delta << k_B T$) almost all of the excitations incident from N propagate into S, so that, in the presence of an external current, a quasiparticle current flows in the superconductor. In the usual situation where the transverse dimensions of the interface are much larger than the London pene-

tration depth, there is no net current in the interior of the superconductor. The internal quasiparticle current is cancelled by a pair current, with a corresponding flow of supercurrent on the surface. The electric field is continuous at the interface, and the electric field, the electric potential, Q*, and the quasiparticle current all decay exponentially into S with a characteristic length λ_{Q*} (see Fig. 25). The boundary resistance is of order $\lambda_{Q*}\rho_s/A$, where ρ_s is the normal-state resistivity of S, and A is the cross-sectional area of the interface. When the temperature is lowered somewhat, a substantial fraction of quasiparticles have energies $\leq\Delta_\infty(T)$, and are Andreév (1964) reflected at or near the NS interface. In this process, a $k_>$ ($k_<$) quasiparticle incident from N is scattered onto the $k_<$($k_>$) branch, and the current carried by these two excitations continues in the superconductor as a supercurrent. Thus, there is no boundary resistance associated with these quasiparticles, and there is a discontinuity in the electric field at the interface (Fig. 25). The potential is continuous at the interface, but its spatial derivative is not. In the presence of a current, the boundary scattering processes introduce disequilibrium in the quasiparticle distributions within an inelastic scattering length on either side of the interface.

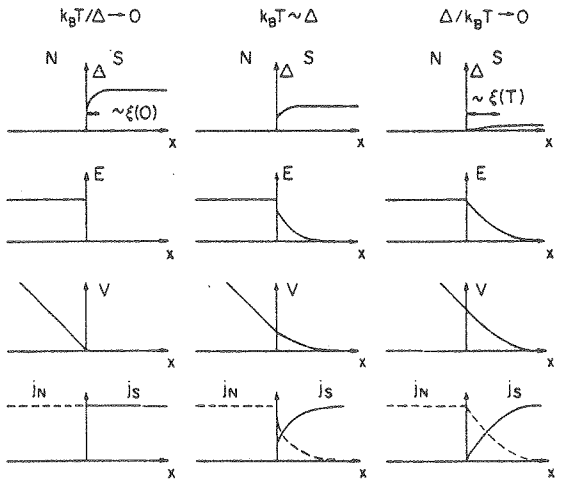

Fig. 25. Variation of energy gap, Δ, electric field, E, electric potential V, normal current, j_N, and supercurrent, j_S, across an NS interface for $k_BT/\Delta \to 0$, $k_BT \sim \Delta$, and $\Delta/k_BT \to 0$. The gap is taken to be zero in N, and the normal state properties are assumed to be the same in the two metals.

As the temperature is lowered still further ($\Delta_\infty >> k_B T$), essentially all of the quasiparticles are Andreév (1964) reflected at the interface, and there is no quasiparticle current in S. Correspondingly, the electric field and potential are zero in S (Fig. 25) and there is no boundary resistance. (In fact, the Andreév scattering process occurs over a distance $\sim\xi_0$, so that the discontinuities in the electric field and the derivative of the potential extend over this region. Furthermore, there will be a small boundary resistance of order $\xi\rho_S/A$ that is negligible in most practical situations.)

We now describe the simple model of HC that is valid in the limit $\Delta_\infty(T) << k_B T$. The model agrees well with the experimental data, and enables one to deduce values of τ_E. We assume that the transition temperature of the normal metal is much less than T, so that we can set $\Delta=0$ for $x<0$ (Fig. 25). In the superconductor, Δ rises from its value at the boundary, $\Delta_o(T)$, to its full value, $\Delta_\infty(T)$, over a distance of roughly the Ginzburg-Landau (1950) coherence length, $\xi(T)$, that is always much less than λ_Q^* in the temperature range investigated experimentally. However, we note that quasiparticles with energies greater than $\Delta_\infty(T)$ may undergo some charge relaxation in the region where Δ varies spatially. At least in the limit $\Delta << k_B T$, this contribution to the overall relaxation rate is likely to be small, and we shall neglect it. We assume that the current densities are sufficiently low that they do not perturb Δ. We further assume that quasiparticles with energies greater than $\Delta_\infty(T)$ are transmitted into S with probability unity; this is a reasonable approximation because of the relatively slow change of Δ with x. Quasiparticles with energies $<\Delta_\infty(T)$ are Andreév (1964) reflected at a plane taken as $x = 0$ [since $\xi(T)<<\lambda_{Q^*}$]. Finally, we assume that the quasiparticles are close to thermal equilibrium even in the vicinity of the interface; we emphasize that this is a reasonable approximation only for $\Delta_\infty << k_B T$.

The charge imbalance generated by the uniform injection of a current I_i into volume Ω of a superconductor in the limit $eV_i << k_B T$ is given from Eqs. (2.24) to (2.26) by

$$Q^* = \frac{Z(T)}{Y(T)} \frac{I_i}{e\Omega} \tau_{Q^*} . \quad (eV_i << k_B T) \tag{6.2}$$

In the case of the NS interface, I_i is just the quasiparticle current injected into S, and is related to the total current, I, by

$$Y(T) = I_i/I. \tag{6.3}$$

Equation (6.3) follows from the realization that in a SIN tunnel junction at low voltages a fraction [1-Y(T)] of the current that flows at T_c cannot flow at a temperature $T < T_c$ because there are no states available in S at energies $<\Delta(T)$, whereas at the NS interface, in our approximation, this same fraction [1-Y(T)] of the total current is transmitted into S as a pair current. Combining Eqs. (6.1) to (6.3), and replacing the exponentially decaying Q* with a value that is constant at the value Q*(0) for $x \leq \lambda_{Q*}$ and 0 for $x > \lambda_{Q*}$, we find

$$Q^*(0) = \frac{Z(T) I \tau_{Q*}}{eA\lambda_{Q*}} . \tag{6.4}$$

The excess voltage, V_b, at each interface of the SNS sandwich adds to the voltage developed across the normal metal, and the total potential across the sandwich is measured with superconducting leads making metallic contact with the superconducting films. This is in contrast to the usual tunneling measurement of Q*, where the potential is measured by a tunneling contact to a normal metal. Thus, we set $g_{NS}(0) = 1$ in Eq. (2.23), and combine the result with Eq. (6.4) to obtain

$$R_b = \frac{V_b}{I} = \frac{Z(T)\lambda_{Q*}\rho_s}{A}, \qquad (\Delta << k_B T) \tag{6.5}$$

In Eq. (6.5) we have set $\tau_{Q*} = 3\lambda_{Q*}^2/\ell v_F$ and used the free electron model (Kittel 1976) to calculate $\rho_s = 3/2e^2 N(0)\ell v_F$. As $T \to T_c$, $Z(T) \to 1$, and the boundary resistance is just the resistance of a length λ_{Q*} of the superconductor in the normal state. As the temperature is lowered, Z(T) decreases, reflecting the fact that fewer quasiparticles are able to propagate into the superconductor. At low temperatures (Clarke et al. 1979) $Z(T) \approx (k_B T/\Delta)^{1/2} \exp(-\Delta/k_B T)$, so that R_b vanishes exponentially as $T \to 0$, as we expect. However, despite the fact that Eq. (6.5) is a good approximation both near T_c and in the limit $T \to 0$, we repeat our caution that it is not expected to be valid at intermediate temperatures where $\Delta_\infty \sim k_B T$.

If one measures R_b near T_c one can, at least in principle, deduce values of τ_{Q*}. As was discussed in Secs. III and V, in general, both inelastic and elastic scattering contribute to

τ_{Q*}^{-1}. We can make a crude estimate of the elastic relaxation rate in the presence of gap anisotropy for the materials used in the experiments to be described by assuming $E \sim k_B T_c$ in Eq. (5.6). This leads us to the conclusion that inelastic scattering should dominate at temperatures above about $0.9T_c$. Since $\Delta/k_B T \simeq 1$ at $T/T_c = 0.9$, it appears that in the range of validity of Eq. (6.5), $\Delta/k_B T \ll 1$, the charge relaxation should be dominated by inelastic scattering, and we assume that $\tau_{Q*} = 4k_B T \tau_E / \pi \Delta_\infty(T)$.

Hsiang and Clarke (1980) measured the resistances of the SNS junctions listed in Table V. Each pair of materials chosen had a low mutual solubility and did not form intermetallic compounds. The PbBi - CuAl samples were made by evaporating the materials onto glass substrates; the CuAl was ~2μm thick, while the PbBi was ~20μm thick, considerably greater than λ_{Q*} over the experimental temperature range. In the remaining samples, the superconductor (up to 80 μm thick) was evaporated onto the two sides of Ir foils about 70 μm thick. The foils were cleaned by sputter etching in argon, the argon was pumped out of the system, and the superconducting material was evaporated onto each side of the foil. Two or three samples were connected in series and their resistances measured with a SQUID voltmeter. The samples were mounted in a vacuum can so that their temperature could be raised above 4.2K. The variation of resistance with temperature is shown in Fig. 26

Table V. Properties of SNS Junctions. The Measured Values of τ_E are Averaged Over 2 or 3 Samples of Each Type.

Superconductor/ normal metal	Type	Measured τ_E (10^{-10}s)	Calculated[a] τ_E (10^{-10}s)
$Pb_{0.99}Bi_{0.01}$-$Cu_{0.97}Al_{0.03}$	film	0.25	0.23(Pb)
Sn-Ir	foil	2.6	2.7
$Sn_{0.99}In_{0.01}$-Ir	foil	1.1	2.7(Sn)
In-Ir	foil	1.1	1.0

a. Kaplan et al. (1976)

for one representative sample of each type. Near T_c, the resistance rises rapidly with increasing temperature, while at low temperatures the resistance is nearly independent of temperature. To within the experimental accuracy, the low temperature resistance

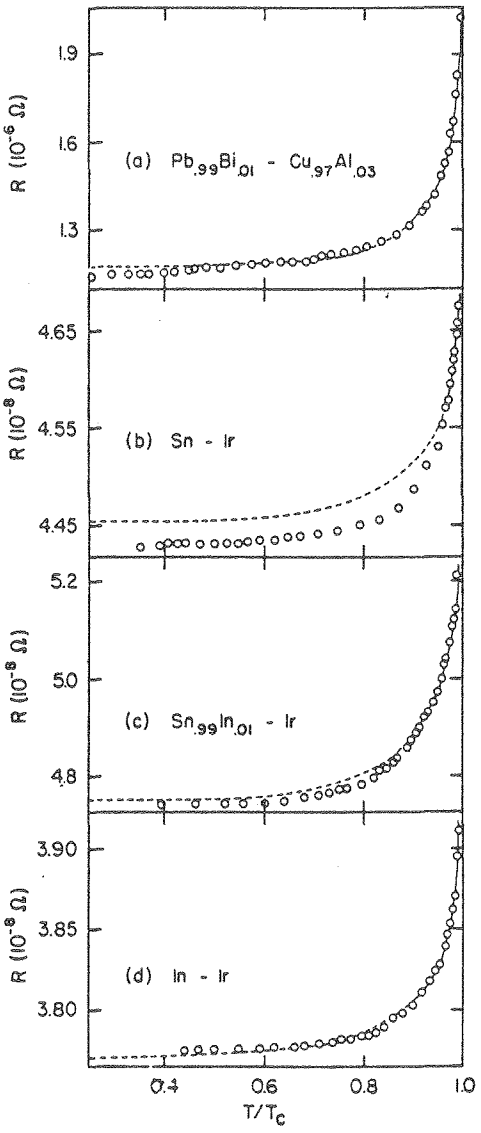

Fig. 26. Circles are measured total resistance vs. T/T_c for SNS junctions listed in Table V. The solid lines above 0.9 T_c [0.96T_c in (b)] are the fit to Eq. (6.5), while the dashed lines show the extrapolation of the theory to lower temperatures.

was equal to the estimated resistance of the normal metal. In fact, an excess resistance equivalent to several mean free paths of the normal metal could not be detected because of the uncertainties in estimating the resistance of the normal layer.

To compare the data with Eq. (6.5), in Fig. 27 we plot the measured resistance vs. $Z(T)(k_BT/\Delta)^{\frac{1}{2}}$. The solid lines are a least squares fit to the data for $T>0.9T_c$ ($0.96T_c$ for Sn). The fit is good -- in fact, for (a), (c) and (d) it is surprising that such good agreement extends down to temperatures as low as $0.9\ T_c$ where $\Delta \sim k_BT$. The slope of the lines in Fig. 26 is $4(\ell v_F \tau_E/3\pi)^{\frac{1}{2}}\rho_s/A$, and

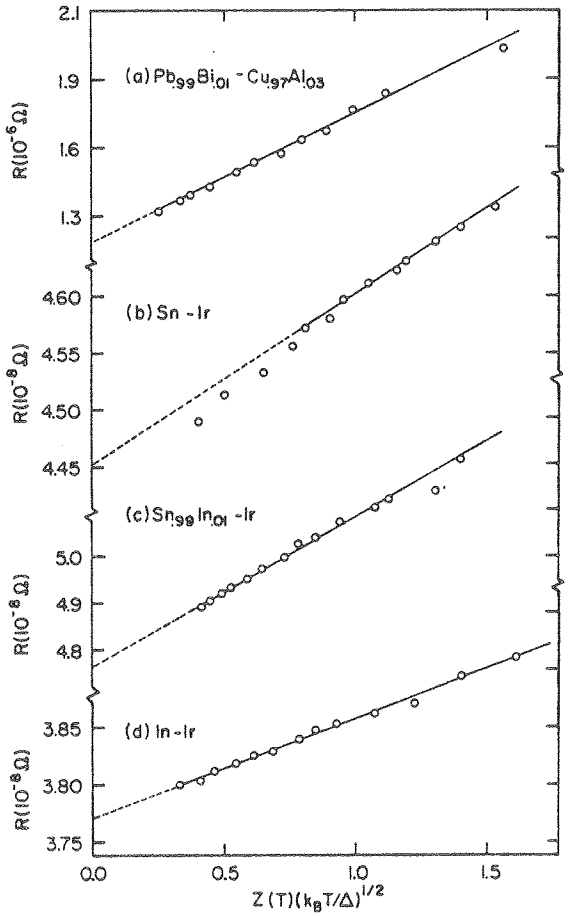

Fig. 27. Total measured resistance vs. $Z(T)(k_BT/\Delta)^{1/2}$ for the samples shown in Fig. 26. The solid lines are a least-squares fit to the data for $T>0.9T_c$ [$0.96T_c$ for (b)].

yields the average values of τ_E listed in Table V. The values of τ_E calculated by Kaplan et al. (1976) from α^2F are also listed for comparison. The agreement is generally quite good. Using the fitted values of τ_E, we have plotted the resistance predicted by Eq. (6.5) in Fig. 26. Except for Sn, the extrapolated low-temperature resistance is in good agreement with the measured resistance, thus providing a good check on the consistency of our results. Particularly in the cases of PbBi and In, the fit is remarkably good even at intermediate temperatures, a result that is probably coincidental, particularly since the expression used for τ_{Q*} is quite inappropriate in this range. However, it may be that the increase in the elastic charge relaxation rate as the temperature is lowered tends to compensate for the decrease in the inelastic rate, thus keeping τ_{Q*} roughly constant at temperatures below about 0.9 T_c. One could, in principle, attempt to fit the data to more detailed theories, for example, that of Waldram (1975), at intermediate temperatures, but the difficulty of accounting for both elastic and inelastic scattering processes and their strong energy dependence makes this a formidable undertaking.

Hsiang (1980) studied the effect of a magnetic field applied parallel to the plane of SNS sandwiches in which the superconductor was $Pb_{0.98}Bi_{0.02}$, and the normal metal was Cd. The PbBi films are bulk, type-II superconductors, and the spin relaxation rate is given by (Maki 1969, de Gennes 1966, Tinkham 1975)

$$\frac{1}{\tau_s} = \frac{\ell v_F eH}{3c} . \qquad (6.6)$$

Hsiang measured the boundary resistance as a function of applied magnetic field and temperature, and extracted values of $\tau_{Q*}^{-1}(T,H)$. Using Eq. (6.6) in Eq. (5.10) he was able to estimate τ_s^{-1} as a function of H. Although there was a good deal of spread in the results, he was able to establish reasonable agreement between the measured value of τ_s^{-1} and the value predicted by Eq. (6.6).

B. Phase-slip Centers

The second topic is the phase-slip center (PSC) in a superconducting filament (Skocpol et al. 1974). Since this topic is covered in detail by Skocpol in Chapter 18, we will discuss it only briefly, emphasizing those aspects involving charge imbalance.

PSC's manifest themselves as steps in the current-voltage characteristics of superconducting whiskers and bridges, usually rather close to T_c, as illustrated in Fig. 28(a). The model of the PSC is shown in Fig. 28(b). As the current, I, is increased eventually it exceeds the critical current at the weakest point in the microbridge. The order parameter in this region collapses to zero and the current is forced to flow as a normal current, thereby allowing the superfluid to build up again and to resume carrying the current. The cycle then repeats at a frequency 2eV/h, where V is the average voltage across the region. Each time the order parameter falls to zero, the phase difference between the two ends of the bridge slips by 2π: Hence the name "phase slip center." The width of the region over which the superfluid oscillates is roughly $2\xi(T)$. Now since the superfluid current oscillates between zero and its critical value, on the average approximately one-half of the current in this region flows as a supercurrent, and the other half as a normal current. One can then regard the PSC as an SNS junction. A fraction of the normal current (depending on temperature) that flows in the phase-slip region will propagate into the superconducting regions on either side, and decay into a supercurrent in a length λ_{Q^*}. Thus, from Eq. (6.5), the apparent resistance generated will be $\sim\frac{1}{2}Z(T)(2\lambda_{Q^*})\rho_s/A$.

Skocpol et al. made samples with several voltage leads. In the example shown in Fig. 28(a), they showed that the first four steps were produced by one PSC forming successively in each of the regions II, I, IV and III, while the fifth step was produced by a second PSC appearing in region IV. The slope, that is, the resistance, of each successive step increases by an approximately constant increment, each increment representing the resistance of one PSC. The only puzzling feature of this original work on PSC's was that the resistance did not appear to diverge as $(T_c-T)^{-\frac{1}{4}}$ as one would expect from the temperature dependence of τ_{Q^*}. However, Dolan and

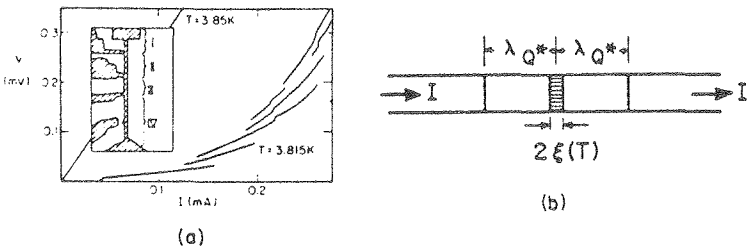

Fig. 28.(a) I vs. V for the whole length of the Sn bridge 140μm long, 4μm wide, and 0.1μm thick shown inset; (b) schematic of PSC in long filament.

Jackel (1977) resolved this difficulty in an elegant experiment in which they prepared a microbridge with a series of superconducting voltage leads along one side of the bridge and a series of normal voltage leads along the other. The probes were typically 2μm apart, and formed tunnel junctions with the microbridge. In this way, they were able to measure the average superfluid and normal potentials, $V_s = \bar{\mu}_s/e$ and $V_N = \bar{\mu}_N/e$, across a PSC, the position of which was defined by a small notch in the microbridge. Figure 29 shows their measured values of V_s and V_N. As expected, V_s changes abruptly, since $\xi(T)$ is less than the probe spacing, while V_N changes over a much greater length. Values of τ_{Q*} deduced from the spatial variation of V_N showed the predicted $(T_c-T)^{-\frac{1}{4}}$ temperature dependence, and produced the value $\tau_{Q*} = 6.3\times10^{9}\ (\Delta/k_B T_c)s^{-1}$, in excellent agreement with the results of Clarke and Paterson (1974) discussed in Sec. IV. Since this work on PSC was performed at $T \geq 0.98T_c$, inelastic scattering should completely dominate the charge relaxation. Thus, the model of the PSC proposed by Skocpol et al. is a complete and satisfying explanation of a phenomenon that had been a puzzle for many years.

More recently, Kadin et al. (1978) studied PSC's in the presence of a magnetic field, H, applied parallel to the Sn strip. By correcting for heating effects, they were able to obtain the expected $(T_c-T)^{-\frac{1}{4}}$ temperature dependence of the resistance near T_c. They also found that the resistance associated with a PSC and hence the inferred value of τ_{Q*} was reduced by the magnetic field. The magnetic field dependence of τ_{Q*}^{-1} was consistent with the prediction of Schmid and Schön [Eq. (5.10)], with (Maki 1969, de Gennes 1966, Tinkham 1975)

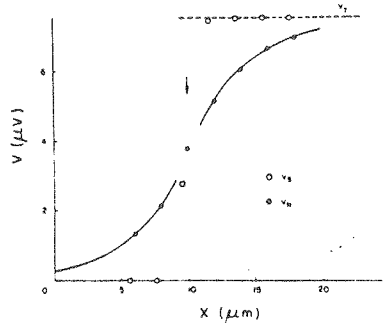

Fig. 29. Spatial variation of V_S and V_N across a PSC in a Sn microbridge at the position marked with the arrow.

$$\frac{1}{\tau_s} = \frac{\Delta(0,0)}{\hbar} \frac{H^2}{H_c{}^2||(0)} \quad . \qquad (6.7)$$

In Eq. (6.7), $\Delta(0,0)$ is the energy gap in zero field at zero temperature, and $H_c||(0)$ is the parallel critical field at zero temperature. This work was the first experimental demonstration of the essential correctness of the SS theory of charge relaxation in a magnetic field.

C. The Flow of Supercurrent in the Presence of a Temperature Gradient

Pethick and Smith (1979a) predicted that when a supercurrent, $\vec{I}$, flows in a superconductor along which there exists a thermal gradient, $\vec{\nabla}T$, a charge imbalance should be created that is proportional to $\vec{I}.\vec{\nabla}T$. Clarke et al. (1979a) observed this effect in Sn films, and established that the measured voltage was proportional to $\vec{I}.\vec{\nabla}T$, as predicted, but two to three orders of magnitude smaller than the predicted value. This discrepancy arose because the theory assumed that the elastic scattering rate was negligible compared with the inelastic rate, whereas the reverse was true in the experiment. Three further theories then appeared (Schmid and Schön 1979, Clarke and Tinkham 1979, and Beyer Nielsen et al. 1980) in attempts to account quantitatively for the temperature dependence and magnitude of the data. More recently, Heidel and Garland (1980) observed similar effects in Al films. I will begin this section by describing the experiment and the results of Clarke et al. (1979a), and then briefly compare the results with the theories. H. Smith and C. M. Falco will also discuss this topic in chapters 15 and 16.

The experimental configuration is shown in Fig. 30. The Sn (or Sn + 3wt.%In) film is typically 300nm thick and 0.1mm wide in the narrow region. After the Sn was oxidized, three Cu(+3%Al) disks $\sim$1μm thick were deposited, followed by three Pb strips. In a given experiment, one of the three Sn-SnOx-Cu tunnel junctions was used to measure the quasiparticle potential relative to the pair potential with a SQUID voltmeter. The substrate was mounted in a vacuum can, with a heater at each end to generate a temperature gradient. The temperature of the junction under investigation and the temperature gradient were estimated from two Allen-Bradley carbon resistors attached to the rear of the substrate.

In the measurements, the creation of a thermal gradient invariably produced a small voltage ($\lesssim$ 1pV). This offset, believed to arise from thermoelectric effects in non-superconducting components in the circuit, was eliminated by defining the voltage to be

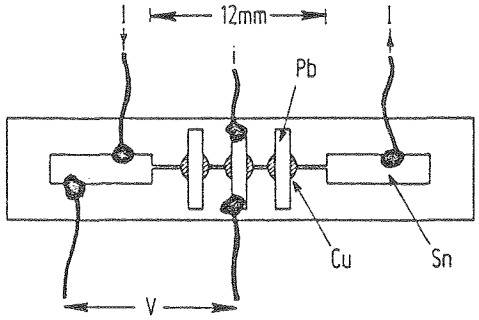

Fig. 30. Sample configuration.

zero when I=0. The current was then increased in steps, and the voltage measured at each step. In Figs. 31 and 32 we plot V vs. I for five values of ∇T, and V vs. ∇T for 10 values of I for a representative sample. Within the experimental accuracy, the voltage is bilinear in I and ∇T. In Fig. 33 we plot $Vg_{NS}(0)/I\nabla T$ vs. $t=T/T_c$. The charge imbalance per unit current and per unit temperature gradient diverges as $T/T_c \to 1$, and falls off steadily with decreasing temperature at low temperatures. To within the experimental resolution, the temperature dependence was the same for all 8 samples investigated. In Fig. 34 we plot $Vg_{NS}(0)/I\nabla T$ vs. (1-t) for the same sample as in Fig. 33; the divergence at temperatures above about $0.8T_c$ is close to $1/(1-t)$. In Table VIwe list the thickness and mean free path of the Sn or SnIn films and the quantity $Vg_{NS}(0)T(1-t) \times A/I\nabla T$ for four samples, two with $\ell > \xi_o$ and two with $\ell < \xi_o$. A is the

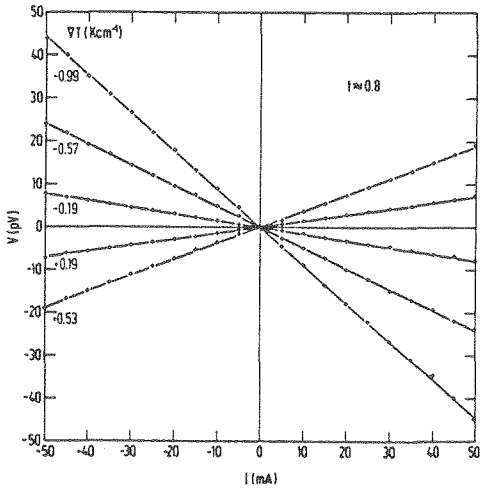

Fig. 31. V vs. I for 5 values of ∇T for sample 4.

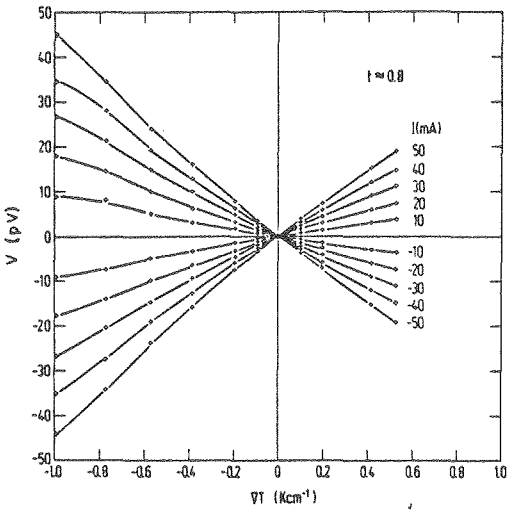

Fig. 32. V vs. ∇T for 10 values of I for sample 4. At each value of ∇T, the voltage is defined to be zero at I=0.

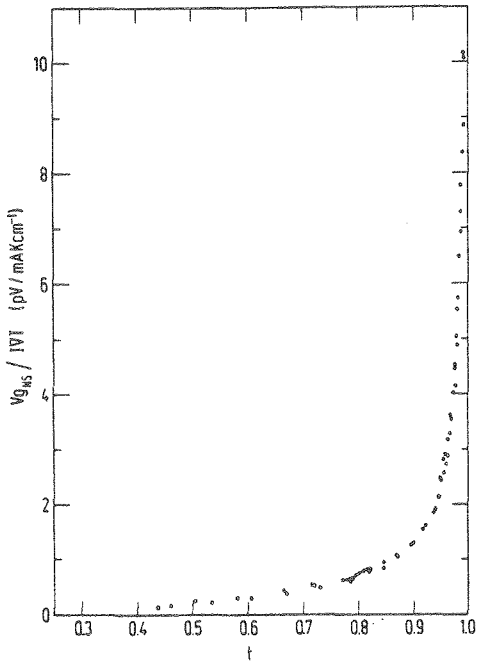

Fig. 33. $Vg_{NS}(0)/I\nabla T$ vs. reduced temperature, t, for sample 4.

cross-sectional area of the films. The results for the two clean samples agree well with each other, as do those for the two dirty samples.

The physical origin of the effect is indicated in Fig. 35. In Fig. 35(a), there is a thermal gradient, but no applied supercurrent. Quasiparticles moving from the left are at an effective temperature $T-\delta T$, while those from the right are at $T+\delta T$, where T is the local temperature. Thus, there is an imbalance in the populations of the $\vec{k}>\vec{k}_F$ and $\vec{k}<\vec{k}_F$ branches on the righthand side of the Fermi surface, but an equal and opposite imbalance on the lefthand side: As a

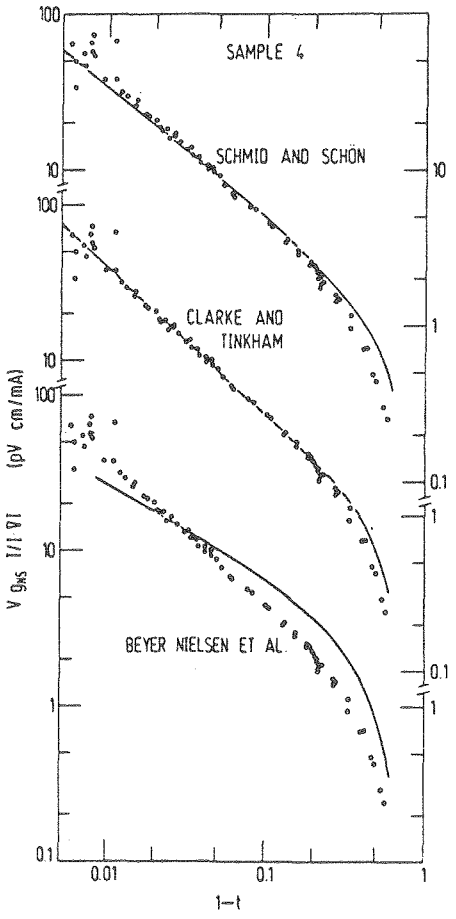

Fig. 34. $Vg_{NS}(0)/IVT$ vs. (1-t) for sample 4. The three theoretical formulas have been fitted to the experiemental data by scaling them appropriately.

Table VI. Properties of 4 Samples

Sample	Material	Thickness (nm)	ℓ (nm)	$Vg_{NS}(0)T(1-t)A/IVT$ ($10^{-16}\Omega cm^3$)
4	Sn	320	428	1.2
6	Sn	430	294	1.0
7	Sn (+3% In)	190	61	0.8
8	Sn (+3% In)	190	61	0.8

result, $Q^*=0$. If we now impose a superfluid velocity $\vec{v}_S$ [Fig. 35(b)] the excitation energies are raised and lowered on opposite sides of the Fermi surface by an amount $\vec{p}_k.\vec{v}_S$ [see Sec. VC]. The induced asymmetry ensures that the population imbalances on opposite sides of the Fermi surface no longer cancel, and the resulting charge imbalance is the origin of the observed voltage.

Since the first paper by Pethick and Smith (1979a), there have been three separate approaches to the calculation of Q^*. Schmid and Schön (1979) gave a result [Eq. (9)] that is valid for both $\ell>\xi_o$ and $\ell<\xi_o$ in the limit $\Delta/k_BT_c\to 0$. However, their formalism is actually valid at all temperatures, and, retroactively, one can readily modify

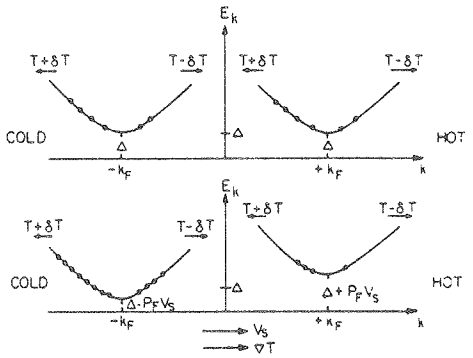

Fig. 35. Schematic representation of quasiparticle excitations in presence of (a) temperature gradient and (b) temperature gradient and applied supercurrent.

their result*. If one uses $\partial f^o/\partial E = -1/4\ k_B T ch^2(\Delta/2k_BT)$ in Eq. (7) in their paper, and inserts the result into Eq. (6), one finds

$$V = \frac{p_F \ell}{6eg_{NS}(0)} \frac{\vec{v}_s.\vec{\nabla}T}{T} \frac{\Delta}{k_BT(1-Z)ch^2(\Delta/2k_BT)} \ln(8\Delta\tau_E/\hbar). \quad (6.8)$$

Here, p_F is the Fermi momentum, and Z is given by Eq. (2.27). Clarke and Tinkham (1980) used a simple kinetic approach to obtain

$$V = \frac{p_F \ell}{6eg_{NS}(0)} \frac{\vec{v}_s.\vec{\nabla}T}{T} \frac{\Delta}{k_BT(1-Z)ch^2(\Delta/2k_BT)} . \quad (6.9)$$

Equation (6.8) exceeds Eq. (6.9) by a factor of $\ln(8\Delta\tau_E/\hbar)$, which varies relatively slowly with temperature over the experimental range studied, with an average value of about 6. This factor is somewhat model dependent. Thus, apart from this factor, the Schmid-Schön and Clarke-Tinkham approaches yield essentially the same result. One can convert v_s into a current density by writing $v_s = j_s/n_s e = \mu_o j_s \lambda^2(T)e/m$, and using the result $\lambda^2(T) = \lambda_L^2(0) \times (1 + \xi_o/\ell)(1-t^4)^{-1}$ (Tinkham 1979) to find

$$v_s = \frac{\mu_o j_s e \lambda_L^2(0)(1 + \xi_o/\ell)}{m(1-t^4)} . \quad (6.10)$$

Near T_c, $1-Z \to \pi\Delta/4k_BT$, $ch^2(\Delta/2k_BT) \to 1$, and $1-t^4 \to 1-t$. Thus, near T_c, the temperature dependence of the voltage at fixed current is dominated by the temperature dependence of v_s, $(1-t)^{-1}$, in good agreement with the experimental results. The curves calculated for the two theories with $v_F = 6.5 \times 10^5 ms^{-1}$, $\lambda_L(0) = 5 \times 10^{-8} m$, and $\xi_o = 2.3 \times 10^{-7} m$ are plotted for sample 4 in Fig. 34. The curves were fitted at $T/T_c = 0.99$ by multiplying Eq. (6.9) by 2.4, and Eq. (6.8) by 0.4. It is evident that both theories predict the observed temperature dependence rather accurately.

Beyer Nielson et al. (1980) and, subsequently, Pethick and Smith (1980) have solved the Boltzmann equation for the case where $\tau_E^{-1} \to 0$ and for an isotropic energy gap to obtain

*G. Schön, private communication

$$V = \frac{p_F \ell}{e g_{NS}(0)} \frac{\vec{v}_s \cdot \vec{\nabla} T}{T} \left[\frac{1.93\Delta/k_B T}{ch^2(\Delta/2k_B T)} + \frac{8/15}{\exp(\Delta/k_B T) + 1} \right] . \quad (6.11)$$

Equation (6.11) is also plotted in Fig. 34, and evidently has a different temperature dependence than the experimental data. In Eq. (6.11), the first term in square brackets dominates the second for $T/T_c \lesssim 0.998$, that is, throughout the experimentally realizable range. The first term arises from quasiparticles in the energy range $\Delta - p_F v_s$ to $\Delta + p_F v_s$ in which the available phase space for charge relaxation via elastic scattering is reduced. This effect is particularly pronounced for quasiparticles with energies near $\Delta - p_F v_s$. However, Schön (1980) has recently suggested that elastic scattering may smear out the energy levels sufficiently to eliminate reduced relaxation rates at low energies, provided that $(p_F v_s/\Delta)^{1/2} << (\hbar/\tau_1)/\Delta$, a restriction that is strongly satisfied experimentally. If this suggestion is correct, the first term in square brackets in Eq. (6.11) will be greatly reduced, and may have a different temperature dependence. The second term is strictly valid only near T_c, and needs to be recalculated to be valid over a wide temperature range.

At the time of writing, these problems are not resolved, but one might reasonably hope for clarification in the very near future. However, it seems clear that an expression of the form of Eq. (6.8) or (6.9) is essentially correct in view of the excellent fit to the data on Sn, as well as to the data on Al obtained by Heidel and Garland.

VII. CONCLUDING SUMMARY

In this chapter I have attempted to develop the main ideas of charge imbalance in superconductors, and its application to various physical situations. We began by introducing the charge imbalance per unit volume, $Q^* = (2/\Omega)\sum_k q_k f_k$, where $q_k = \xi_k/E_k$ is the effective quasiparticle charge. Charge imbalance is tunnel injected at the rate $Q_i^* = F^* I_i/e\Omega$, where F^* is a known function of V_i and T. The steady state charge imbalance, $Q^* = \dot{Q}_i^* \tau_{Q^*}$, where $\tau_{Q^*}^{-1}$ is the charge relaxation rate, produces a voltage $V = Q^*/2N(0)e\, g_{NS}(0)$ measured at zero detector current by a tunneling contact to a normal metal. In the absence of magnetic scattering or gap anisotropy, charge relaxation occurs via inelastic scattering at the rate $(F^* \tau_{Q^*})^{-1} = \pi\Delta(T)/4k_B T_c$ in the limit $\Delta/k_B T \to 0$. All of these results may be taken as exact.

Elastic scattering can relax charge imbalance under several different circumstances. If the gap anisotropy is non-zero, the coherence factor $(uu'-vv')^2$ for branch crossing is no longer zero. A computer solution of the appropriate Boltzmann equation yields results in good agreement with experiments on Al, using the normalized mean-square gap anisotropy as a fitting parameter. The presence of magnetic impurities can greatly enhance $\tau_{Q^*}^{-1}$ because the coherence factor for branch crossing $(uu'+vv')^2$, approaches unity at low energies. Experimental data obtained on Al doped with Er is in excellent agreement with the Schmid-Schön prediction $(F^*\tau_{Q^*}^{-1}) = [\pi\Delta(T)/4k_BT_c\tau_E](1 + 2\tau_E/\tau_S)^{\frac{1}{2}}$ over a wide range of values of τ_E/τ_S for $\Delta/k_BT_c \lesssim 0.8$. This is a very surprising result, since the theory is valid only for $\Delta/k_BT_c \ll 1$. On the other hand, however, a computer solution of the Boltzmann equation with the appropriate magnetic scattering term yields results that differ strikingly from the data. Charge relaxation can also be induced by a supercurrent in the film: The current induces an asymmetry across the Fermi surface that again allows branch relaxation via elastic scattering. The results from experiments on dirty Al are again in excellent agreement with the Schmid-Schön result, but in disagreement with the results of the computer calculation. Thus, charge relaxation in the presence of a pair breaking mechanism is in urgent need of attention, both because the Boltzmann equation produces results that are in distinct disagreement with the data, and because the Schmid-Schön theory is valid over a much wider temperature range than can reasonably be expected.

Finally, we discussed three other types of experiments involv- charge imbalance. The first was the resistance of the NS interface in the clean limit. A simple modification of the tunneling theory for the injection of Q* yields a result that is in excellent agreement with experiments on Pb, Sn, and In, and that produces very reasonable values of τ_E. The next example was the phase-slip center in a narrow superconducting strip. The magnitude of the resistance increment generated by each PSC is well explained by the theory of the NS interface. Finally, a charge imbalance is generated by the flow of a supercurrent in the presence of a temperature gradient. Theories by Schmid and Schön (1979) and by Clarke and Tinkham (1980) are in good agreement with data obtained from Sn and Al, while a theory by Beyer Nielsen et al. (1980) is in disagreement. Certain aspects of the theory of the effect, notably the relaxation rate of quasiparticles at low energies, remain to be explained.

In conclusion, I should like to point out that there are a number of other situations involving charge imbalance that I have not described in this chapter. These include branch imbalance waves

(see chaps. 18 and 19), the existence of a temperature gradient in a superconductor (chap. 16) or across a NS interface, and the prediction that the charge relaxation rate near T_c in a pulsed measurement should be essentially τ_E^{-1} rather than $\tau_E^{-1}(\Delta/k_B T_c)$ (Kadin et al. 1979). These topics seem likely to receive considerable attention in the near future.

ACKNOWLEDGEMENTS

Much of the work described here was carried out in collaboration with others, namely C. C. Chi, U. Eckern, B. R. Fjordbøge, T-Y Hsiang, T. R. Lemberger, P. E. Lindelof, J. L. Paterson, A. Schmid, G. Schön, and M. Tinkham, to all of whom I express my grateful thanks. In addition I should like to thank J-J Chang, O. Entin-Wohlman, R. Orbach, A. B. Pippard, C. J. Pethick, D. J. Scalapino, H. Smith, D. J. Van Harlingen, and J. R. Waldram for helpful discussions. T. R. Lemberger and D. J. Van Harlingen made innumerable constructive suggestions during the writing of the manuscript, and H. J. Mamin carefully read the final version and eliminated a number of errors.

This work was supported by the Division of Materials Sciences, Office of Basic Energy Sciences, U.S. Department of Energy under Contract Number W-7405-ENG-48.

REFERENCES

Abrikosov, A. A., and Gor'kov, L. P., 1960, Contribution to the theory of superconducting alloys with paramagnetic impurities, Zh. Eksp. Teor. Fiz., 39:1781 [Sov. Phys. JETP, 12:1243].

Anderson, P. W., 1959, Theory of dirty superconductors, J. Phys. Chem. Solid., 11:26.

Andreev, A. F., 1964, The thermal conductivity of the intermediate state in superconductors, Zh. Eksp. Teor. Fiz., 46:182 [Sov. Phys. JETP, 19:1228].

Aronov, A. G., 1974, The influence of condensate motion on the thermoelectric effects in superconductors, Zh. Eksp. Teor. Fiz., 67:178 [Sov. Phys. JETP, 40:90].

Artemenko, N., and Volkov, A. F., 1977, Andreev reflection and the electric resistance of superconductors in the intermediate state, Zh. Eksp. Teor. Fiz., 72:1018 [Sov. Phys. JETP, 45:533].

Artemenko, N., Volkov, A. F., and Zaiteev, A. V., 1978, On the contribution of the superconductor resistance of a superconductor-normal metal system, J. Low Temp. Phys., 30:487.

Bergmann, G., 1971, Eliashberg function $\alpha^2(E)F(E)$ and the strong-coupling behavior of a disordered superconductor, Phys. Rev., B3:3797.

Beyer Nielsen, J., Ono, Y. A., Pethick, C. J., and Smith, H., 1980, The effect of impurity scattering on the thermally induced charge imbalance in a clean superconductor, Solid State Comm., 33:925.

Blackford, B. L., 1976, A tunneling investigation of energy-gap anisotropy in superconducting bulk aluminum crystals, J. Low Temp. Phys., 23:43.

Chambers, R. G., 1952, The anomalous skin effect, Proc. Roy. Soc. Lond., 215:481.

Chang, J-J, 1979, Relaxation of the quasiparticle charge imbalance in superconductors, Phys. Rev., B19:1420.

Chang, J-J, and Scalapino, D. J., 1977, Kinetic-equation approach to nonequilibrium superconductivity, Phys. Rev., B15:2651.

Chi, C. C., and Clarke, J., 1979, Quasiparticle branch mixing rates in superconducting aluminum, Phys. Rev., B19:4495.

Chi, C. C., and Clarke, J., 1980, Addendum to "Quasiparticle branch mixing rates in superconducting aluminum," Phys. Rev., B21:333.

Chi, C. C., and Langenberg, D. N., 1976, Microwave response of non-equilibrium superconductors, Bull. Am. Phys. Soc., 21:403.

Clarke, J., 1972, Experimental observation of pair-quasiparticle potential difference in nonequilibrium superconductors, Phys. Rev. Lett., 28:1363.

Clarke, J., 1976, Superconducting quantum interference devices for low frequency measurements in: "Superconductor Applications: SQUIDS and Machines," B. B. Schwartz and S. Foner, eds., Plenum, New York.

Clarke, J., Eckern, U., Schmid, A., Schön, G., and Tinkham, M., 1979, Branch-imbalance relaxation times in superconductors, Phys. Rev., B20:3933.

Clarke, J., Fjordbøge, B. R., and Lindelof, P. E., 1979a, Supercurrent induced charge imbalance measured in a superconductor in the presence of a thermal gradient, Phys. Rev. Lett., 43:642.

Clarke, J., and Paterson, J. L., 1974, Measurements of the relaxation of quasiparticle branch imbalance in superconductors, J. Low Temp. Phys., 15:491.

Clarke, J., and Tinkham, M., 1980, Theory of quasiparticle charge imbalance induced in a superconductor by a supercurrent in the presence of a thermal gradient, Phys. Rev. Lett., 44:106.

Craven, R. A., Thomas, G. A., and Parks, R. D., 1971, Sharpening of the resistive transition of a superconductor with the addition of paramagnetic impurities, Phys. Rev., B4:2185.

DeGennes, P. G., 1964, Boundary effects in superconductors, Rev. Mod. Phys., 36:225.

DeGennes, P. G., 1966, "Superconductivity of metals and alloys," Benjamin, New York.

Dolan, G. J., and Jackel, L. D., 1977, Voltage measurements within the non-equilibrium region near phase slip centers, Phys. Rev. Lett., 39:1628.

Entin-Wohlman, O., and Orbach, R., 1979, Effect of pair breaking on branch relaxation in nonequilibrium superconductors, Phys. Rev., B19:4510.

Fickett, F. R., 1971, Cryogenics, 11:349.

Galperin, Yu. M., Gurevich, V. L., and Kozub, V. I., 1974, Thermoelectric effects in superconductors, Zh. Eksp. Teor. Fiz., 66:1387 [Sov. Phys. JETP, 39:680].

Ginzburg, V. L., and Landau, L. D., 1950, Zh. Eksp. Teor. Fiz., 20:1064.

Gray, K. E., Long, A. R., and Adkins, C. J., 1969, Measurements of the lifetime of excitations in superconducting aluminum, Phil. Mag., 20:273.

Gschneidner, K. A., 1964, Physical properties and interrelationships of metallic and semi-metallic elements, Solid State Phys., 16:275.

Harding, G. L., Pippard, A. B., and Tomlinson, J. R., 1974, Resistance of superconducting-normal interfaces, Proc. Roy. Soc. Lond., A340:1.

Heidel, D. F., and Garland, J. C., 1980, Thermoelectric potentials in superconducting aluminum films, Bull. Am. Phys. Soc., 25:411.

Hsiang, T-Y, 1980, Magnetic field dependence of the superconductor-normal metal boundary resistance, Phys. Rev., B21:956.

Hsiang, T-Y, and Clarke, J., 1980, Boundary resistance of the superconducting-normal interface, Phys. Rev., B21:945.

Kadin, A. M., Skocpol, W. J., and Tinkham, M., 1978, J. Low Temp. Phys., 33:481.

Kadin, A. M., Smith, L. N., and Skocpol, W. J., 1980, Charge imbalance waves and nonequilibrium dynamics near a superconducting phase-slip center, J. Low Temp. Phys., 38:497.

Kaplan, S. B., Chi, C. C., Langenberg, D. N., Chang, J. J., Jafarey, S., and Scalapino, D. J., 1976, Quasiparticle and phonon lifetimes in superconductors, Phys. Rev., B14:4854.

Kittel, C., 1976, "Introduction to Solid State Physics," 5th edition, Wiley, New York.

Knorr, K., and Barth, N., 1970, Superconductivity and phonon spectra of disordered thin films, Solid State Comm., 8:1085.

Krähenbühl, Y., and Watts-Tobin, R. J., 1979, Microscopic theory of the current-voltage relationship across a normal-superconducting interface, J. Low. Temp. Phys., 35:569.

Lawrence, W. E., and Meador, A. N., 1978, Calculation of the order-parameter relaxation times in superconducting aluminum, Phys. Rev., B18:1154.

Leavens, C. R., and Carbotte, J. P., 1971, Contribution to the theory of weak coupling superconductors, Can J. Phys., 49:724; 1972, Gap anisotropy in a weak coupling superconductor, Annals of Physics, 70:338.

Lemberger, T. R., and Clarke, J., 1980, Charge-imbalance relaxation in the presence of a pair-breaking interaction in superconducting AlEr films, submitted to Phys. Rev. B.

Lemberger, T. R., and Clarke, J., 1980a, Charge imbalance relaxation in the presence of a pair-breaking supercurrent in dirty, superconducting films, submitted to Phys. Rev. B.

Long, A. R., 1973, The attenuation of high frequency phonons in metals, J. Phys., F3:2023.

Maki, K., 1969, Gapless superconductivity, in: "Superconductivity," R. D. Parks, ed., Marcel Dekker, New York.

Markowitz, D., and Kadanoff, L. P., 1963, Effect of impurities upon critical temperature of anisotropic superconductors, Phys. Rev., 131:563.

Meservey, R., and Schwartz, B. B., 1969, Equilibrium properties: comparison of experimental results with predictions of the BCS theory, in: "Superconductivity," R. D. Parks, ed., Marcel Dekker, New York.

Moody, M. V., and Paterson, J. L., 1979, Relaxation of the distribution function branch imbalance Q* in Sn and Sn-In alloys, J. Low Temp. Phys., 34:83.

Ovchinnikov, Yu. N., 1977, Penetration of an electrical field into a superconductor, J. Low Temp. Phys., 28:43.

Pethick, C. J., and Smith, H., 1979, Relaxation and collective motion in superconductors: a two-fluid description, Annals of Physics, 119:133.

Pethick, C. J., and Smith, H., 1979a, Generation of charge imbalance in a superconductor by a temperature gradient, Phys. Rev. Lett., 43:640.

Pethick, C. J., and Smith, H., 1980, Charge imbalance in nonequilibrium superconductors, to be published in J. Phys. C.

Pippard, A. B., 1965, "The Dynamics of Conduction Electrons," Gordon and Breach, New York.

Pippard, A. B., Shephard, J. G., and Tindall, D. A., 1971, Resistance of superconducting-normal interfaces, Proc. Roy. Soc. Lond., A324:17.

Rieger, T. J., Scalapino, D. J., and Mercereau, J. E., 1971, Charge conservation and chemical potentials in time-dependent Ginzburg-Landau theory, Phys. Rev. Lett., 27:1787.

Rothwarf, A., and Taylor, B. N., 1967, Measurement of recombination lifetimes in superconductors, Phys. Rev. Lett., 19:27.

Schmid, A., and Schön, G., 1975, Linearized kinetic equations and relaxation processes of a superconductor near T_c, J. Low Temp. Phys., 20:207.

Schmid, A., and Schön, G., 1979, Generation of branch imbalance by the interaction between supercurrent and thermal gradient, Phys. Rev. Lett., 43:793.

Schön, G., 1980, unpublished.

Schuller, I., and Gray, K. E., 1977, Temperature dependence of the relaxation time of the superconducting order parameter, Solid State Comm., 23:337.

Skocpol, W. J., Beasley, M. R., and Tinkham, M., 1974, Phase-slip centers and nonequilibrium processes in superconducting tin microbridges, J. Low Temp. Phys., 16:145.

Smith, L. N., and Mochel, J. M., 1976, Phonon and quasiparticle dynamics in superconducting aluminum tunnel junctions, Phys. Rev. Lett., 35:1597.

Tinkham, M., 1972, Tunneling generation, relaxation, and tunneling detection of hole-electron imbalance in superconductors, Phys. Rev., B6:1747.

Tinkham, M., 1975, "Introduction to Superconductivity," McGraw-Hill, Inc., New York.

Tinkham, M., and Clarke, J., 1972, Theory of pair-quasiparticle potential difference in non-equilibrium superconductors, Phys. Rev. Lett., 28:1366.

Van Harlingen, D. J., 1980, Thermoelectric generation of charge imbalance at superconductor interfaces, Bull. Am. Phys. Soc., 25:411.

Waldram, J. R., 1975, Chemical potential and boundary resistance at normal-superconducting interfaces, Proc. Roy. Soc. Lond., A345:231.

Yu, M. L., and Mercereau, J. E., 1972, Electric potentials near a superconducting-normal bondary, Phys. Rev. Lett., 28:1117.

Zavaritzkii, N. V., 1969, Increase of the critical temperature of superconductors condensed at low temperatures, Zh. Eksp. Teor. Fiz., 57:752 [Sov. Phys. JETP, 30:412].